Maaze *et al. Int J Concr Struct Mater* (2025) 19:35
https://doi.org/10.1186/s40069-025-00767-3

International Journal of Concrete Structures and Materials

RESEARCH

Open Access

Economic-Environmental and Multi-Criteria Optimization for Predicting Alkaline Ratios in Waste Cement Concrete-Based Geopolymer Using Central Composite Design

Mohammed Rihan Maaze[1], Sourav Kumar Das[2*], Nikhil Garg[3] and Sandeep Shrivastava[4]

Abstract

India, as the world's second-largest cement producer, faces significant environmental challenges due to high carbon emissions from cement production. This study investigates the potential of using waste cement concrete (WCC) powder as a sustainable precursor in geopolymer concrete, aiming to advance sustainable development and effective waste management. Utilizing a central composite design (CCD) approach, the research optimizes molarity (M) and alkaline mix (AM) ratios to enhance the material's properties. Findings reveal that heat curing increases the 28-day compressive strength by 15–20% compared to room-temperature curing. Moreover, environmental impact assessments indicate a 15% reduction in Global Warming Potential (GWP) and a 12% reduction in Acidification Potential (AP), despite a 30% higher fossil fuel (FF) impact due to alkali use compared to traditional Portland cement mortar. Multi-response desirability analysis identifies the optimal molarity (10) and alkaline mix ratio (2.5) for achieving balanced performance across compressive strength, water absorption, shrinkage, tensile bond strength, and GWP. The confirmation experiments validate these predictive models, showing close alignment between predicted and observed values, ensuring the reliability and accuracy of the optimization approach. The study concludes that geopolymer mortars, particularly those cured at 60 °C with a 10 M NaOH solution and the optimal alkaline ratio, offer an environmentally friendly and mechanically superior alternative to conventional cement mortars. This approach supports sustainability by reducing environmental impact, promoting effective waste management, and contributing to sustainable development in the construction industry.

Keywords Geopolymer mortar, Environmental assessment, Central composite design, Construction and demolition waste

Journal information: ISSN 1976-0485 / eISSN 2234-1315.

*Correspondence:
Sourav Kumar Das
souravkumar.das@jaipur.manipal.edu
Full list of author information is available at the end of the article

1 Introduction

According to the 2011 census, 377 million Indians were living in the metropolitan area; by 2050, that number is expected to rise to 800 million (Census of India, 2011; United Nations, 2018). This massive rise in the urban population subsequently increases the demand for housing and will eventually increase the construction industry's consumption of concrete cement. India stands as the second-largest cement manufacturer globally, second only to China. The cement manufacturing process, primarily through clinker production, leaves a massive carbon footprint, posing significant environmental challenges. The construction industry is increasingly exploring innovative solutions to reduce its environmental impact in response to these challenges. One promising approach is the utilization of by-products or secondary materials to develop new adhesives, such as geopolymers. Geopolymers represent a class of inorganic polymers formed by the chemical activation of aluminosilicate materials with alkaline solutions. These materials offer a more environmentally friendly alternative to traditional Portland cement, known for its high carbon emissions. The production of geopolymers can incorporate various waste materials, thus addressing both environmental sustainability and waste management issues.

The exponential growth in the urban population in India is a significant driver for the construction industry. Urbanization leads to increased demands for residential, commercial, and industrial infrastructure. As the population in metropolitan areas balloons, so does the need for new housing developments. This development is not just limited to new constructions; it also encompasses renovating and retrofitting existing structures to accommodate the growing urban populace. These activities inevitably lead to substantial construction and demolition (C&D) waste, with a significant portion being waste cement concrete (WCC).

The generation of C&D waste poses a significant challenge. The heterogeneity of C&D waste—concrete, bricks, wood, metals, glass, plastics, and more—makes recycling difficult. Unmanaged disposal of C&D waste consumes valuable landfill space and poses environmental risks due to the contamination of soil and groundwater from hazardous substances contained in the waste. Besides building new houses, renovation and retrofitting of old structures will also increase a substantial amount of construction and demolition (C&D) waste, among which the majority will be waste cement concrete (WCC). Furthermore, C&D waste is difficult to recycle due to its huge heterogeneity, and unmanaged unloading of C&D waste consumes a large amount of landfill space and poses a threat to the environment because of the varying levels of contamination of these wastages (Bossink & Brouwers, 1996; Formoso et al., 2002). Finding sustainable ways to manage and recycle C&D waste is critical. Effective waste management mitigates the environmental impact and contributes to resource conservation by recycling valuable materials. Recognizing the challenges and opportunities presented by C&D waste, many government organizations worldwide are encouraging its use in construction. Policies and incentives are being introduced to promote recycling C&D waste into construction materials. These measures aim to reduce the construction industry's environmental footprint and better use the waste materials generated from construction and demolition activities. Many studies have been conducted on using C&D waste as a substitute for natural aggregates in concrete production. Research has demonstrated that C&D waste, when processed and used appropriately, can produce concrete properties comparable to those made with natural aggregates. This not only helps in reducing the demand for natural resources, but also addresses the problem of C&D waste disposal (S. Ismail & Ramli, 2013; Malešev et al., 2010; Poon & Lam, 2008).

One of the significant innovations in using C&D waste is the development of geopolymers. Geopolymers are produced by the alkaline activation of aluminosilicate materials, which can include a variety of industrial by-products, such as fly ash and slag, as well as C&D waste materials like clay bricks, cement concrete, and glass. Geopolymers have been found to offer superior strength and durability compared to traditional cement mixtures (Hillier et al., 1999; Marinković et al., 2010; Parthiban et al., 2017; Sagoe-Crentsil et al., 2001). Fly ash and slag are typically used waste materials in the production of geopolymers; however, C&D waste materials such as clay brick, cement concrete, and glass are also being investigated (Ahmari et al., 2012; Das & Shrivastava, 2021a; El-Wafa & Fukuzawa, 2018; N. Ismail & El-Hassan, 2018; Zaharaki et al., 2016). Research has shown that geopolymers made from C&D waste materials perform well in terms of mechanical properties and contribute to better environmental outcomes. The inclusion of waste materials rich in calcium oxide (CaO), such as slag or certain types of C&D waste, can enhance the formation of both sialate link and calcium silicate hydrate (CSH) gels, which are crucial for the strength and durability of the geopolymer matrix (Ahmari et al., 2012; Buchwald et al., 2007; Yip et al., 2005). This study focuses on the potential of using waste cement concrete (WCC) powder as a precursor for geopolymer production. By leveraging WCC, the research aims to provide a sustainable solution to the growing problem of construction and demolition (C&D) waste, which is becoming increasingly prevalent due to rapid urbanization and infrastructure development.

Curing regimes of geopolymers have always been an influential factor. Several studies have examined how curing temperature affects the quality and durability of geopolymers made from different precursors. Allahverdi and Kani (2009) studied the utilization of clay brick and cement concrete waste as precursors and reported an 8 M NaOH mixture with curing temperature ranging from 60 to 80 ℃ as optimum. Another study by Robayo et al. (2016) reported 70 ℃ as an optimum temperature while clay brick and cement are used as precursors, which is in line with the previous one. Another study utilizing cement concrete waste as 100% precursor material with 6% Na_2O content resulted in a compressive strength of 11.64 MPa by heat curing at 70℃ for the first 24 h of casting (Robayo-Salazar et al., 2017). Komnitsas et al. (Komnitsas et al., 2015) reported that 100% concrete waste geopolymers cured at 90 °C for 7 days had a crushing strength of 13 MPa. Another study by C. Lampris et al. (2009) with the collected silts from different C&D waste sites in the United Kingdom, reported that a 9 M NaOH solution mixture when cured at 60℃ for 3 days achieved a crushing strength of 25 MPa after 7 days of casting.

From the literature review, clay brick was found to be the most investigated precursor for geopolymer manufacture among all C&D waste, including concrete, glass, ceramic, and tableware. Different heat curing regimens were tested, yielding similar results. Thus, this study examined how heat curing affects the compressive strength of geopolymer mortar mixtures prepared from 100% WCC powder cured at five different temperature ranges starting from 30 ℃ to 70 ℃, with an increment of 10 ℃ for a wide range of molarity and alkali mixture ratios. The research seeks to develop geopolymer mortars that offer superior mechanical properties and reduced environmental impact by optimizing the curing conditions and mix proportions.

To gain a thorough understanding of the research landscape concerning the use of waste concrete in geopolymer concrete, a bibliometric analysis was conducted using VOS viewer. This tool systematically evaluates the field, revealing key research trends and identifying gaps. Initially, data collection was performed using Boolean logical operators (AND/OR) across topics (TOPIC), abstracts (ABS), and keywords (KEY). The specific search query employed was "Geopolymer Concrete" AND "recycled concrete powder" (TOPIC), yielding a database of 182 documents for analysis. This examination, covering publications from 2003 to 2023, highlighted a significant under-exploration of waste concrete powder utilization in geopolymer concrete (Fig. 1). Subsequently, the search query was refined to "waste-based Geopolymer Concrete" AND "optimize" (TOPIC), resulting in a database of 93 documents. The bibliometric analysis indicated that

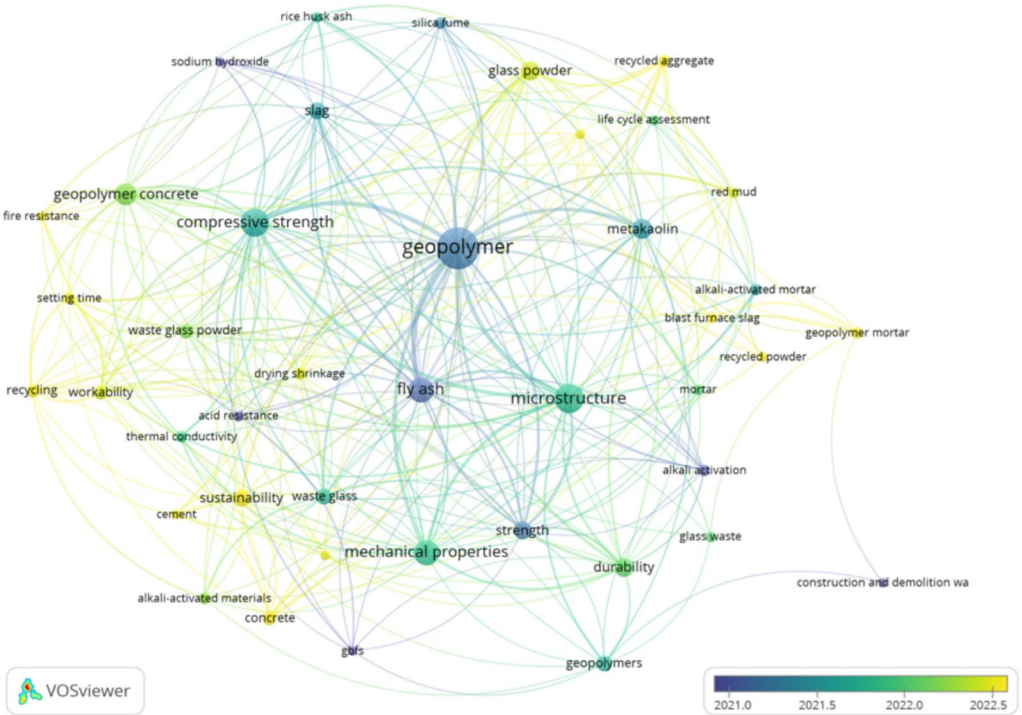

Fig. 1 Bibliometric analysis of author's keywords visualized using VOS viewer for Query 1

only a limited number of studies have addressed optimization, marking it as an emerging area of interest for researchers (Fig. 2). The analysis highlighted two critical observations:

1. **Limited exploration of WCC powder:** Despite its potential, the utilization of waste cement concrete powder in geopolymer applications has received minimal attention in academic research. This gap underscores the need for dedicated studies to unlock its capabilities.
2. **Emerging interest in optimization:** Optimization methods in geopolymer concrete research, particularly involving waste-based materials, are gaining traction. However, most studies have concentrated on traditional industrial by-products like fly ash and slag, with limited focus on C&D waste materials.

These findings position the current study as a pivotal contribution to the field. By leveraging bibliometric insights, the research emphasizes the novelty of integrating WCC powder into geopolymer mortar and applying advanced optimization techniques to achieve balanced performance metrics. The bibliometric results, visually represented in Figs. 1 and 2, illustrate the evolving focus of research trends. The analysis indicates that optimization has been addressed in only a limited number of studies, highlighting it as an emerging area of interest for researchers.

The literature review consolidates findings from recent studies on recycled concrete aggregates, sustainable geopolymer concrete, and geopolymer bricks, emphasizing the optimization methods employed to enhance material properties. One notable study by Ghazy (2020); Ghazy, (2020) examines the performance of geopolymer bricks (GB) incorporating recycled concrete aggregates (RCA), marble powder (MP), and limestone powder (LP) using the Taguchi method. The L16 orthogonal array reduces the number of experiments and facilitates result analysis. The study evaluates density, mechanical properties (compressive and flexural strengths) at 28 days, and water absorption percentage. Findings reveal that combining RCA, MP, and LP can produce geopolymer bricks with 36–58 MPa compressive strengths at ambient temperature. RCA significantly influences the performance of the bricks, making them suitable for environmentally friendly construction comparable to those made with natural aggregates.

The latest study by Singh and Rajhans (2024) (Singh & Rajhans, 2024) investigates the mechanical properties of geopolymer concrete (GPC) prepared with treated

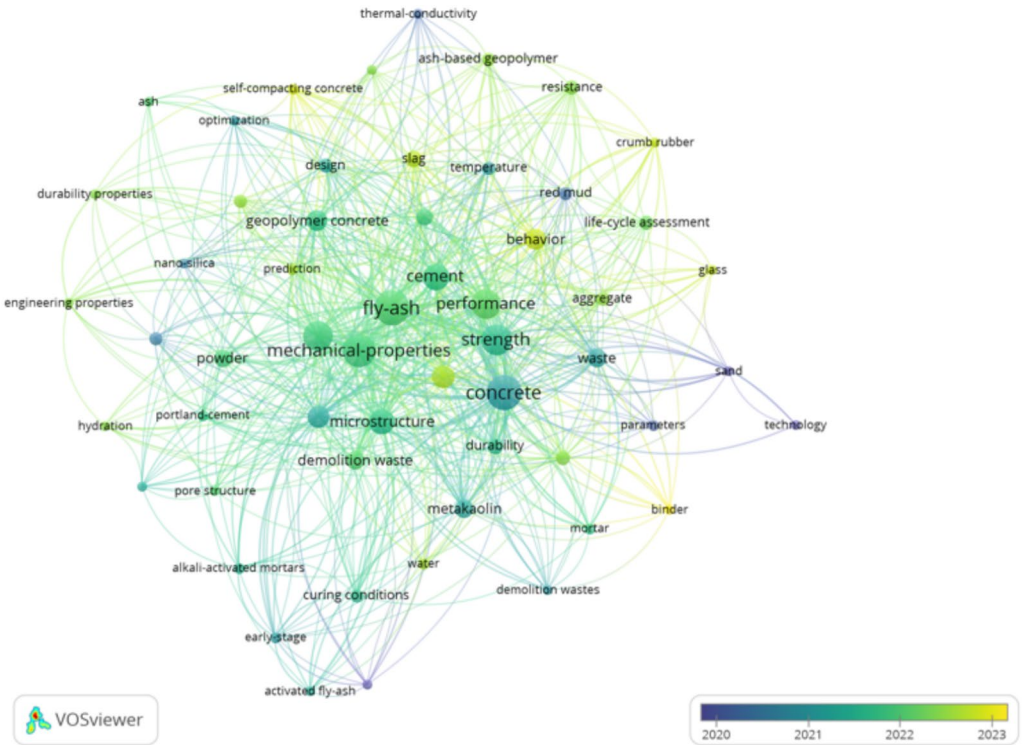

Fig. 2 Bibliometric analysis of author's keywords visualized using VOS viewer for Query 2

recycled concrete aggregate (RCA) using a modified two-stage mixing approach (M-TSMA(sp-ggbs)). The study utilizes fly ash (FA) and ground granulated blast slag (GGBS) as cement alternatives, partially replacing FA with silica powder (SP). The RCA is treated with sodium silicate to improve the adhered mortar's strength. Bayesian optimization combined with Support Vector Regression (SVR) and Gaussian Process Regression (GPR) models predict the mechanical strengths of GPC mixtures. Results indicate significant improvements in RCA's physical and mechanical characteristics, with enhanced mechanical strengths of GPC mixes. The SVR and GPR models accurately predict these strengths, demonstrating the effectiveness of machine learning algorithms in optimizing construction material properties.

The reviewed studies highlight the significant potential of using optimization methods to improve the performance and sustainability of construction materials incorporating recycled and industrial waste. The application of Bayesian optimization with SVR and GPR models, as well as the Taguchi method, demonstrates how advanced optimization techniques can substantially enhance material properties. These methods support the development of sustainable construction practices, promoting the use of recycled materials in industry. Future research should continue to refine these optimization techniques and explore new applications to reduce the environmental impact of construction activities further. This finding emphasizes the need for focused research on optimizing the molarity and alkaline ratios in geopolymer concrete using waste concrete, utilizing advanced statistical methods such as central composite design (CCD) and Bayesian Optimization. The current study employs the central composite design (CCD) approach to optimize the molarity and alkaline ratio for the geopolymer mixtures. This statistical method allows for estimating quadratic terms and interaction effects between the factors, providing a comprehensive analysis of their influence on the response variables. In addition to mechanical performance, the study also assesses the environmental impacts of the produced geopolymer mixtures. The environmental assessment focuses on three key indicators: global warming potential (GWP), acidification potential (AP), and fossil fuel (FF) depletion. By comparing these impacts with those of conventional Portland cement mortars, the study aims to highlight the environmental benefits of using geopolymers.

2 Materials and Methodology

2.1 Raw Materials and Mixing Process

WCC was collected from a local demolition site. The collected WCC was plain cement concrete slabs of different sizes which were being pulverized from a commercial crushing plant. No chemical treatment was done before pulverizing the material and the grounded WCC was being used in its original chemical condition in this study. Figure 3a depicts a SEM image of the waste cement concrete (WCC) powder, whose surface morphology is rough and heterogeneous, with irregular particle shapes. The microstructural analysis reveals the presence of several mineral phases dispersed in the matrix. Elemental composition of WCC powder is presented in Fig. 3b, which gives Energy Dispersive X-ray Spectroscopy (EDS) results. The primary elements identified are oxygen (O), silicon (Si), calcium (Ca) and aluminum (Al), while there are also minor amounts of iron (Fe), potassium (K) and sulfur (S). X-ray diffraction (XRD) pattern of the WCC powder (Fig. 3c) shows that it contains a number of crystalline phases such as quartz (Q), albite (A), anorthite (An), Calcite (C) and portlandite (P). These phases are essential during geopolymerization processes. Quartz increases strength and stabilizes the structure of geopolymer matrix. For geopolymer formulation, aluminosilicate framework is formed by combination of albite and anorthite. In geopolymers, a calcium carbonate compound called calcite can alter the time taken for it to set plus its strength. By providing additional calcium hydroxide, Portlandite can react with silicates to produce calcium silicate hydrate (CSH) gels that enhance mechanical properties.

The particle size distribution (PSD) of WCC powder (refer Fig. 3d) indicates a wide range of particle sizes, with a significant proportion being fine particles. The median particle size (D50) is 19.56 microns, suggesting a high surface area. This is beneficial for the geopolymerization reaction as it enhances the dissolution rate of aluminosilicate precursors in the alkaline solution. The fine particle size of WCC powder ensures high reactivity, which is essential for efficient geopolymerization, resulting in a denser and stronger geopolymer matrix. The fine aggregates used in this study were river sand which fits well within the upper and lower limit for Zone-II grade of sand as specified by Indian Standards IS:2116-1980 (BIS:2116 1980). A complete mix proportion is shown in Table 1 which implies quantities of the precursor, fine aggregate, and alkali solutions. In this study, a mixture of sodium hydroxide (lab grade with a purity of 98%) solution and sodium silicate (commercial grade with a chemical composition of $Na_2O = 8.40\%$, $SiO_2 = 27.22\%$ and $H_2O = 64.38\%$) solution was utilized.

In this experimental program to determine the effect of different heat curing temperature on the compressive strength, the dry combination was first produced by mixing fine aggregate and precursor in a Hobart mixture. For homogeneity, the dry mixing was continued for 4 min and then the alkali solution was combined with the dry

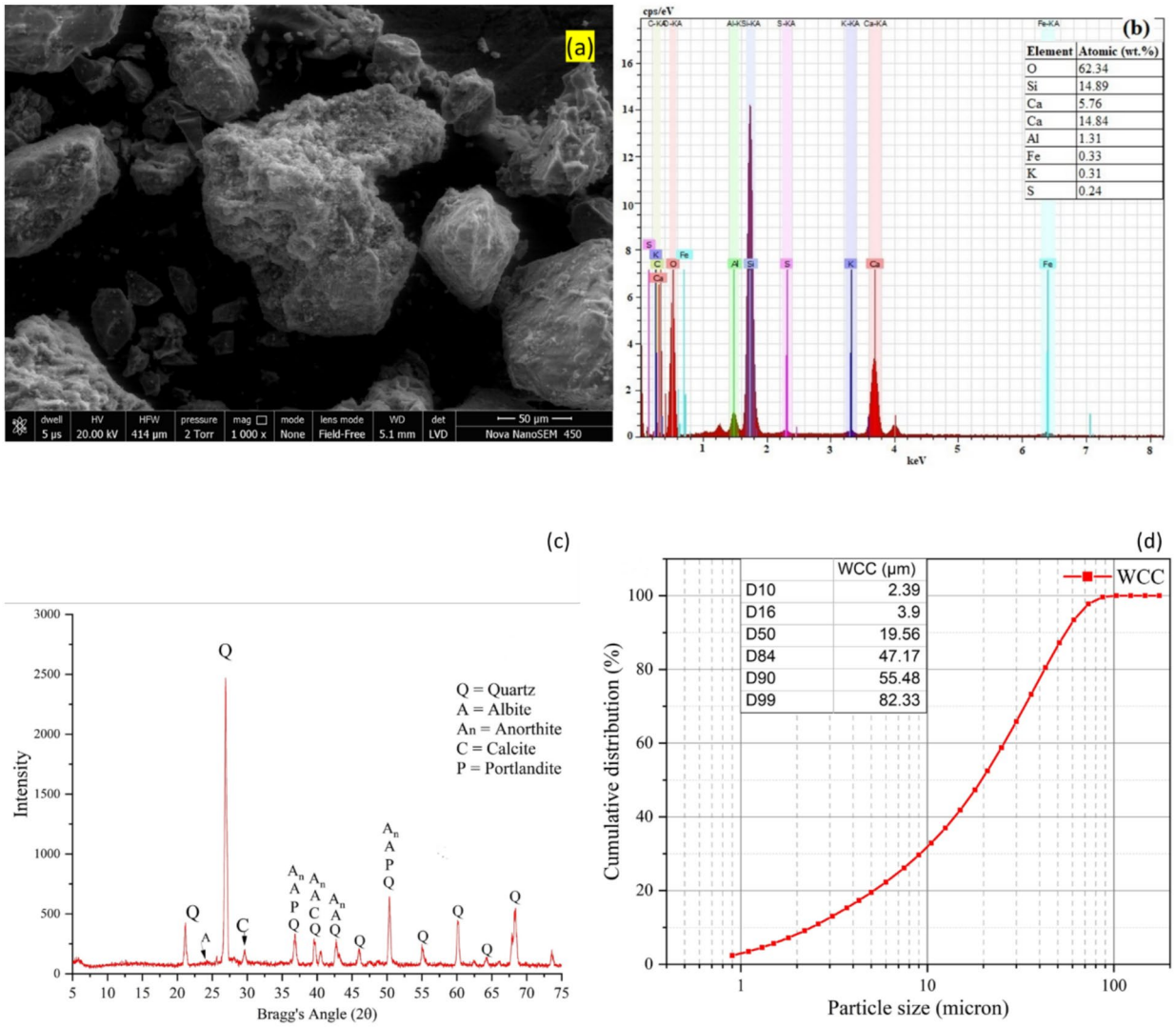

Fig. 3 **a** FESEM image, **b** EDS mapping, **c** XRD pattern, **d** particle size distribution of WCC powder (Das & Shrivastava, 2021b)

mixture with further mixing being continued by 3 min to achieve homogeneity. The fresh mixture was poured into a 50 mm^3 mold and vibrated in a table vibrator for two minutes to evacuate any entrapped air. For 24 h, the molds were stored in a 25 ℃, 50% relative humidity laboratory. Then after 24 h of casting, specimens were demoulded and placed in a temperature-controlled oven at specified test temperatures of 30 ℃, 40 ℃, 50 ℃, 60 ℃, and 70 ℃ for 24 h. After 48 h of casting, the specimens were moved to a 30 ℃, 85 ± 5% relative humidity chamber for resting before testing.

2.2 Central Composite Design and Methodology

The central composite design (CCD) is a widely used experimental design in response surface methodology (RSM), particularly useful for fitting a quadratic surface to understand the interaction between variables and optimize responses. CCD involves a factorial or fractional factorial design with center points and a group of 'star points' that allow for the estimation of curvature. For this study, two factors are considered: A: molarity and B: alkaline ratio. The levels of these factors are determined based on preliminary experiments or prior knowledge. The CCD will include factorial points, which are a full or fractional factorial design, center points where all factors are set to their mid-levels, and axial (star) points that are at a distance 'α' from the center, allowing the estimation of quadratic terms (Table 2). These components ensure a comprehensive analysis of the effects of the factors on the response variable.

Table 1 Experimental mix for the mechanical property evaluation

Sl. no.	Symbol*	WCC (kg/m^3)	Fine aggregate (kg/m^3)	NaOH pellet (kg/m^3)	Na_2SiO_3 solution (kg/m^3)	Na_2O (% of binder mass)	Silicate modulus
1	6M1.5AM	507	1520	32	244	11.2	1.45
2	8M1.5AM	507	1520	40	244	12.7	1.28
3	10M1.5AM	507	1520	47	244	14	1.16
4	12M1.5AM	507	1520	53	244	15.2	1.07
5	14M1.5AM	507	1520	59	244	16.3	0.99
6	16M1.5AM	507	1520	64	244	17.3	0.94
7	6M2.5AM	507	1520	23	290	10.4	1.86
8	8M2.5AM	507	1520	28	290	11.5	1.68
9	10M2.5AM	507	1520	34	290	12.5	1.54
10	12M2.5AM	507	1520	38	290	13.3	1.45
11	14M2.5AM	507	1520	42	290	14.1	1.37
12	16M2.5AM	507	1520	46	290	14.8	1.30
13	6M3.5AM	507	1520	18	316	10	2.10
14	8M3.5AM	507	1520	22	316	11	1.91
15	10M3.5AM	507	1520	26	316	11.6	1.81
16	12M3.5AM	507	1520	30	316	12.3	1.71
17	14M3.5AM	507	1520	33	316	12.9	1.63
18	16M3.5AM	507	1520	36	316	13.4	1.57

*Symbol, 6 M means 6 molarity of NaOH solution and 1.5AM means 1.5 alkali mixture (Na_2SiO_3 solution / NaOH solution) ratio

Table 2 Coded values with face centered central composite design for optimization

Run	Standard run	Coded values		Uncoded values		Na_2SIO_3 Solution (kg)	NaOH Solution (kg)	Na_2O %	SiO_2 %	H_2O %
		Molarity	Alkaline mix ratio	Molarity	Alkaline mix ratio					
1	7	−1	−1	6	1.5	60	40	12.85	17.11	70.05
2	12	1	−1	16	1.5	60	40	31.22	15.17	53.61
3	1	−1	1	6	3.5	77.8	22.2	10.42	20.91	68.67
4	5	1	1	16	3.5	77.8	22.2	16.82	20.42	62.77
5	13	−1	0	6	2.5	71.4	28.6	12.13	21.20	66.67
6	10	−1	0	16	2.5	71.4	28.6	13.42	23.45	63.14
7	2	0	−1	12	1.5	60	40	22.45	18.74	58.82
8	9	0	1	12	3.5	77.8	22.2	14.87	21.45	63.68
9	8	0	0	12	2.5	71.4	28.6	17.85	21.21	60.94
10	6	0	0	12	2.5	71.4	28.6	17.85	21.21	60.94
11	3	0	0	12	2.5	71.4	28.6	17.85	21.21	60.94
12	11	0	0	12	2.5	71.4	28.6	17.85	21.21	60.94
13	4	0	0	12	2.5	71.4	28.6	17.85	21.21	60.94

Fig. 4 depicts a 3D surface plot illustrating the relationship between molarity (A) and alkaline ratio (B) on the standard error of design. The plot includes design points (indicated by red dots), which represent specific experimental conditions tested. The contour lines at the base of the plot show the standard error values across different combinations of molarity and alkaline ratio. The surface itself is shaded to represent the varying levels of standard error, with lighter areas indicating lower standard error and darker areas indicating higher standard error.

2.3 Experimental Methodology

2.3.1 Compressive Strength

The compressive strength results presented in this article is the mean of three tested specimens from each batch. All specimens were tested for compressive strength at 0.9

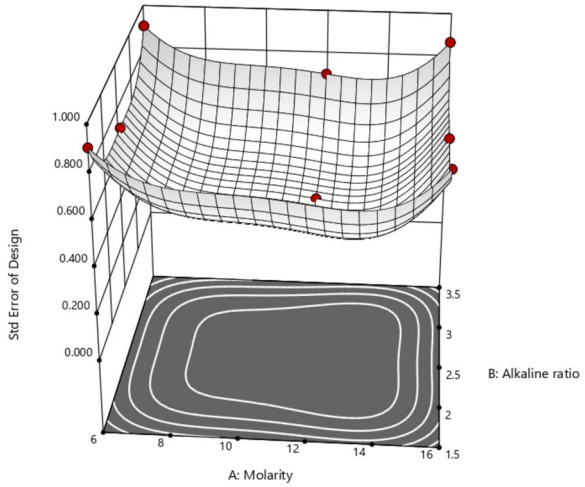

Fig. 4. 3D surface plot illustrating the relationship between molarity (**A**) and alkaline ratio (**B**)

kN/s to 18 kN/s utilizing servo-controlled universal testing equipment according to ASTM C109/109 M [31].

2.3.2 Drying Shrinkage

The drying shrinkage test was carried out on five prisms of size 25×25×285 mm for each batch of mixture. The process followed to do the drying shrinkage test is mentioned in ASTM C1148 (2014), and the automated length comparator used in the study has the least count of 0.001 mm. Now, after demolding the specimen after 48 h of casting, the first reading was taken at 3 days of casting, and that reading is taken as the reference reading for all other successive readings for each specimen.

2.3.3 Sorptivity

As per ASTM C1403, three 50 mm cubes of each of the eighteen mixes were used to measure the water absorption rate by capillarity. After 28 days of curing, the samples were dried for 24 h at 110 ± 5℃, and the weight was recorded. The samples were then kept on a steel mesh in a container with 90% of the exposed surface visible. The water was filled in the container up to 3 mm depth. After adding water, the samples were wiped dry with damp cloth after every 0.25, 1, 4, and 24 h to measure their weight. After each reading, the samples were returned to their original containers immediately.

2.3.4 Tensile Bond Strength

The tensile bond strength of bricks and mortar samples for each mix combination was measured using brick couplets. This test was performed according to ASTM C952 (2002). Before the test, clay bricks were soaked for 24 h. A square mold measuring 92×13×13 mm was set at the center of the brick, and the mortar was poured into it. The mold was then eliminated from the mortar bed. A second brick was laid on top of the mortar bed perpendicular to the brick placed at the bottom. The frame of the drop hammer was placed on top of the brick and dropped from a height of approximately 40 mm. After curing for 28 days following the process mentioned in ASTM C952 (2002), the samples were put between the two tripods. The arrangement was placed in a compression testing machine, and the load was applied. The sample must fail within two minutes of the initial load is applied.

2.4 Life Cycle Assessment

In practice, building designers choose sustainable materials and solutions to maximize their construction businesses. Also, interest is shown in economic sustainability where investors seek strategies to promote their investments while reducing environmental consequences (Gomes et al., 2020; Ortiz et al., 2009). Depending on the amount of detail requirements, a product's life cycle assessment (LCA) might include more or fewer activities which are considered as the boundaries of LCA (Farinha et al., 2019; Jiménez et al., 2015). The "Cradle to gate" approach is considered in this experimental study, as illustrated in Fig. 5.

Now, life cycle inventory (LCI) measures energy and raw material needs, air and waterborne emissions, solid wastes, and other discharges for a product, process, or activity conducted within its life cycle. This step includes collecting data and calculating a product's inputs and outcomes. Environmental Product Declarations (EPD), site-specific data, scientific research, or worldwide databases may be used to create the inventory. The LCA impact assessment follows the inventory. The LCI assessment quantifies the human health and environmental

Fig. 5 Development process of LCA (Khodabakhshian et al., 2018)

impacts of the LCI's environmental resources and discharges. The LCA's final part is interpreting the findings. In the interpretation step, the findings are evaluated, and a preferable product, method, or service is chosen, considering uncertainties and assumptions (Farinha et al., 2019).

2.4.1 Impact Categories for Environmental Assessment

In this study, assessments of the environmental impacts of the utilization of waste on the produced mortars were conducted upon various criteria, viz., the global warming potential, acidification potential, and fossil fuel eradication for the cradle-to-gate boundary condition. Hence, the LCI data related to GWP (CO_2-eq per kg) are calculated based on the material collection and processing phase depending on the transportation of the materials from the collection site where CO_2 emission due to diesel burning is calculated from the www.dieselnet.com database ("Emission Standards: India, On-Road Vehicles and Engines" n.d.); electricity consumption due to two-stage crushing and grinding of the materials at the processing plant and conversion of that consumed electricity to equivalent CO_2 emission (GOI-MOP, 2019); and finally return to the institute laboratory through transportation. Regarding crushing and grinding of the collected waste, initially, the collected WCC is supplied into a D-crusher for reducing the particle size to 20 mm down, where the D-crusher consumed 2.2 kWh to crush the WCC. In the second stage of processing through grinding, a pulverizer was utilized which consumed 10 kWh energy to produce particle size of 90 microns down. In total, 2200 kg of WCC was collected from the source for processing, and after the two-stage processing, 1850 kg of WCC was returned to the institute laboratory. Regarding transportation, a single 4-wheeler of Bharat stage-IV emission rating was hired to collect and return the processed waste from the collection site to the institute laboratory. The entire transportation process was done on a single trip with varying distances between the points of interest. Finally, the electric energy consumed during mixing, the vibration of the mortars, and heat curing are calculated in terms of kilowatt-hour (kWh), and its equivalent CO_2 was computed. Other impact categories, viz., acidification potential (AP) and fossil fuel (FF) eradication data, are obtained from literature. The process flow diagram for the environmental assessment is shown in Fig. 6

The life cycle inventory (LCI) data regarding the GWP of the materials comprising the emission from transportation, crushing, and grinding at the crushing plant and transfer back to the institute laboratory per kg of material are presented in Table 3. Data collected from literature for other impact categories for a particular material are tabulated in Table 4.

The environmental score is an index score that is computed by normalizing the GWP, AP, and FF individual index scores. As all three-index categories are essential,

Table 3 Calculated value of GWP (CO_2-eq per kg) for WCC

Material	Transportation	Two-stage processing	Total
WCC	0.0049	0.0079	0.0128

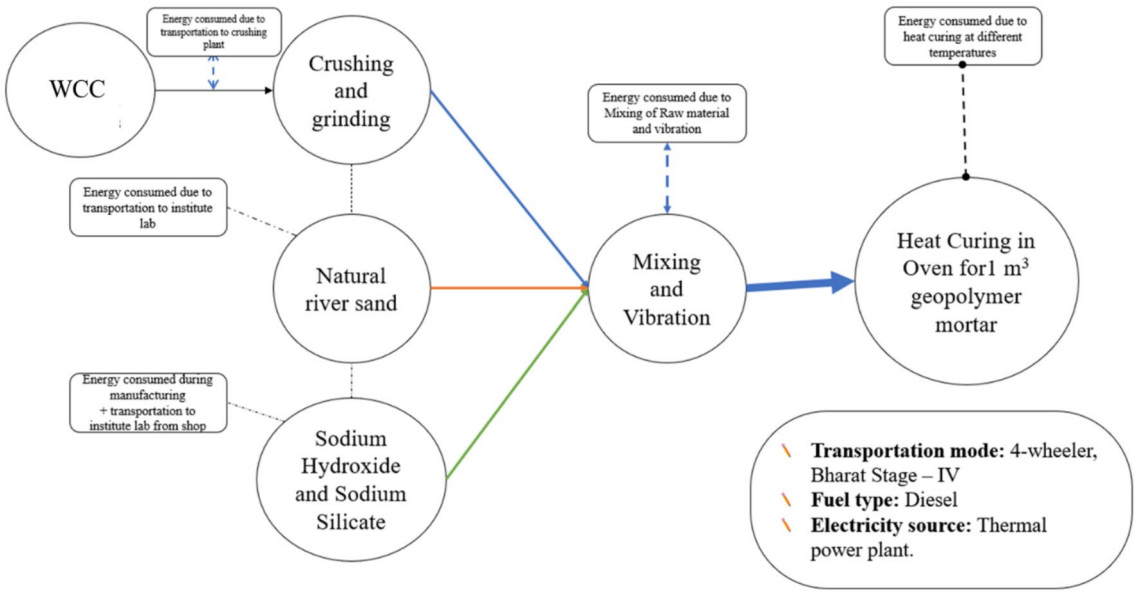

Fig. 6 Process flow diagram

Table 4 Reference LCI data for the constituents of the geopolymer mortars

Constituents	Impact categories			
	GWP (CO_2-eq per kg)	AP (SO_2-eq per kg)	FF (MJ per kg)	Ref
WCC	–	0.00000338	0.005	(Brito, 2021)
Sand	0.0032	0.00002	0.006	(Khodabakhshian et al., 2018)
NaOH	1.39	0.00283	16.000	(Meshram & Kumar, 2022)
Na_2SiO_3	0.6967	0.00507	8.370	(Meshram & Kumar, 2022)
Cement	0.859	0.0053	6.090	(Prakasan et al., 2020) (Meshram & Kumar, 2022)

all the categories were given the same weightage. The environmental score is calculated using Eq. 1 (Lippiatt, 2000):

$$\text{EnvScore}_i = \sum_{k=1}^{p} \text{IAScore}_{ik}, \quad (1)$$

where EnvScore_i is the i^{th} alternative's environmental performance score; p is the number of EI categories and IAScore_{ik} is the alternative i^{th} weighted and normalized impact assessment score in terms of environmental effect k. The IAScore_{ik} is calculated using Eq. 2:

$$\text{IAScore}_{ik} = \frac{\text{IA}_{ik} \times \text{IV}_{wtk}}{\text{Max}\{\text{IA}_{1k}, \text{IA}_{2k}, \ldots, \text{IA}_{mk}} \times 100, \quad (2)$$

where IV_{wtk} = importance weight for k^{th} impact; m = product alternatives; IA_{mk} = Raw IA score for option 'm' with k^{th} environmental effect.

The environmental assessment was conducted by calculating the GWP, AP, and FF index scores for each mortar mixture at the production stage. For evaluation of the produced geopolymer mortar's environmental impacts, the environmental impacts of the conventional 1:3 cement mortar (356 kg OPC 43 grade and 1517 kg zone-II river sand) are taken as reference. For the entire environmental assessment, a total of 19 mixtures have been taken into consideration out of which 18 mixes were 100% WCC powder-based geopolymers of varying molarity and alkali mixture ratio, and one conventional cement mortar of 1:3.

2.5 Economic Analysis

For an economic analysis of the geopolymer masonry mortars produced, two different aspects have been considered which are:

- Material procurement and processing cost per kg
- Electricity consumption for heat curing.

The material procurement and processing cost are presented in Table 5, where all the materials are listed, and their total price per kg is mentioned. For comparison with conventional cement mortar, the cost of cement is included in the list. Table 6 presents the cost incurred for the production of per cubic meter of geopolymer mortar and cement mortar. The heat curing was conducted in a 330-L volume temperature-controlled hot oven and Table 7 shows the cost incurred for different curing temperatures per cubic meter of mortar preparation which has been adjusted in Table 6 during cost calculation.

3 Results and Discussion

3.1 Effect on Compressive Strength

The effect of heat curing on the prepared samples evaluation as conducted by heat curing the samples for 24 h just after demolding. Five different temperature zone were identified, viz., 30, 40, 50, 60 and 70 ℃, and the samples were cured at the specified temperature and left to cool down after 24 h of heating and further placed at 30℃ for the rest curing age. Figure 7 illustrates the variation in the compressive strength due to heat curing. According to Fig. 7, the most critical parameters for compressive strength development is the molarity of NaOH solution and curing age. High alkalinity, which also has a significant concentration of Na^+ cations, promotes the dissolution of Si and Al from the aluminosilicate source. On the other hand, excess hydroxide (OH^-) ions cause early

Table 5 Cost of different materials, including their procurement and processing (lab scale)

Items	Cost per kg (USD $)
WCC powder	0.0088
Sand	0.014
NaOH pellets	0.52
Na_2SiO_3 solution	0.10
Cement	0.088

Table 6 Cost of production per cubic meter of geopolymer mortar (lab scale)

Mix ID	Cost per cum (USD $)	Mix ID	Cost per cum (USD $)	Mix ID*	Cost per cum (USD $)
6M1.5AM	64.75	6M2.5AM	64.69	6M3.5AM	64.70
8M1.5AM	68.89	8M2.5AM	67.28	8M3.5AM	66.77
10M1.5AM	72.51	10M2.5AM	70.38	10M3.5AM	68.84
12M1.5AM	75.62	12M2.5AM	72.45	12M3.5AM	70.91
14M1.5AM	78.72	14M2.5AM	74.52	14M3.5AM	72.47
16M1.5AM	81.31	16M2.5AM	76.59	16M3.5AM	74.02
Cement mortar*	49.40				

*Mix ratio considered for cement mortar is 1:3

Table 7 Electricity cost per cubic meter volume of mortar

Temperature	Electricity consumption within 24 h by 330-L volume hot oven (kwh)	Total cost for 1 m^3 of mortar curing (USD $)
40℃	2.86	2.74
50℃	3.36	3.21
60℃	4.35	4.16
70℃	5.32	5.08

precipitation of aluminosilicate and restricts the availability of Si and Al in the mixes for geopolymerization at various curing ages.

When compared between the different alkali mixture ratio (AM) mix combinations, it was observed that different AM groups reported optimum strength for different molarity mixtures, like 1.5AM group reported optimum for 16 M molarity, 2.5AM group for 10 M molarity and 3.5AM group for 12 M molarity. In addition, when considering the effect of various curing temperature ranges, temperature of 60 ℃ was found as the ideal temperature for geopolymerization. However, a low or too-high molarity not only fails to dissolve the optimal level of Si and Al ions from the WCC, but a high-temperature curing (above 60 °C) for 24 h also creates a hindrance in the geopolymerization process, as observed for 1.5AM and 2.5AM mixture group where the 28-day strength decreases for 70 ℃ curing temperature. Other researchers have also mentioned a similar phenomenon (Görhan & Kürklü, 2014). Therefore, based on experimental data, it could be concluded that the most conducive environment for the geopolymerization of WCC is 10 M NaOH solution with 2.5AM along with heat curing at 60 °C for 24 h.

Now, analyzing the percental increment of the compressive strength (Fig. 7d–f), mixtures cured at a controlled temperature of 30℃ reported less percental change in their early days (3 to 28 days) compressive strength. Also, lower molarity mixtures reported the highest percental change in compressive strength, which depicts delayed compressive strength generation due to delayed geopolymerization activity. After heat curing the samples almost achieved approximately 50%, 60%, and 55% of their 28 days compressive strength within the initial 3 days of casting for 1.5AM, 2.5AM, and 3.5 AM mixture group, respectively. Within 7 days, the samples achieved almost 70%, 80%, and 78% of their 28-day compressive strength. The possible reason behind this phenomenon is the creation of an optimal environment for geopolymer chain formation at an early age. Comparing the controlled temperature and heat-cured samples, samples cured at 60℃, reported a higher percental increment in compressive strength at the initial curing age. However, at 28 days, the compressive strength gain was within a zone of 15–20% only.

3.2 Drying Shrinkage

Fig. 8 illustrates the shrinkage values of waste cement concrete-based geopolymer mortar over 180 days. Initially, all mixes exhibit a rapid increase in shrinkage values within the first 25 days. Mixes with higher alkaline mix (AM) ratios (e.g., 2.5 and 3.5) tend to show higher initial shrinkage compared to those with lower AM ratios (1.5). This higher shrinkage can be attributed to the increased concentration of sodium silicate in the alkaline solution, which accelerates the geopolymerization process, leading to more rapid water loss and subsequent shrinkage. After 25 days, the rate of shrinkage begins to stabilize for most mixes. Mixes such as 6M1.5AM, 8M1.5AM, and 10M1.5AM show a slower rate of shrinkage increase compared to their higher AM ratio counterparts. However, higher AM ratio mixes (16M2.5AM and 16M3.5AM) continue to exhibit significant shrinkage, indicating ongoing internal changes. By 90 days, the shrinkage values for most mixes start to plateau, suggesting that the majority of shrinkage has occurred.

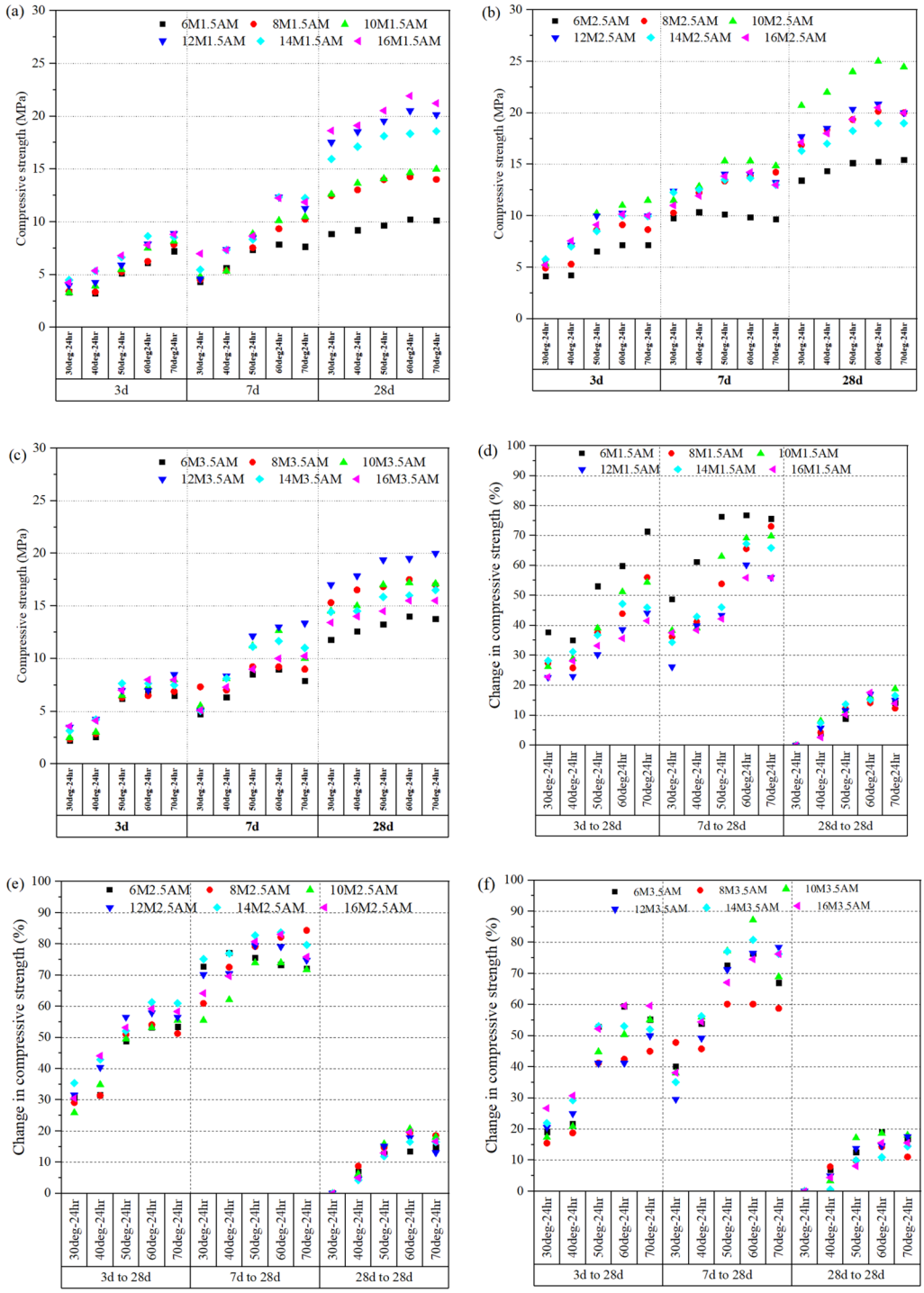

Fig. 7 Change in compressive strength for different alkali content and curing age (**a**, **b** and **c**) and percental change in compressive strength (**d**, **e** and **f**)

Mixes with 3.5 AM ratios demonstrate more pronounced long-term shrinkage, indicating that higher AM ratios could lead to greater overall dimensional changes due to the continued reaction and reorganization of the geopolymer matrix. Notably, mixes such as 14M2.5AM and 16M2.5AM show the highest shrinkage values. This could be due to the combined effects of high molarity and AM ratios, where the higher molarity of the NaOH

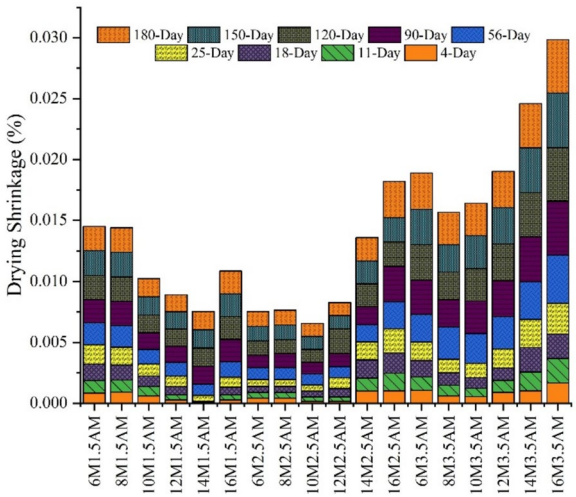

Fig. 8 Shrinkage values for WCC-based geopolymer mortar with varying molarity and alkaline mix ratio

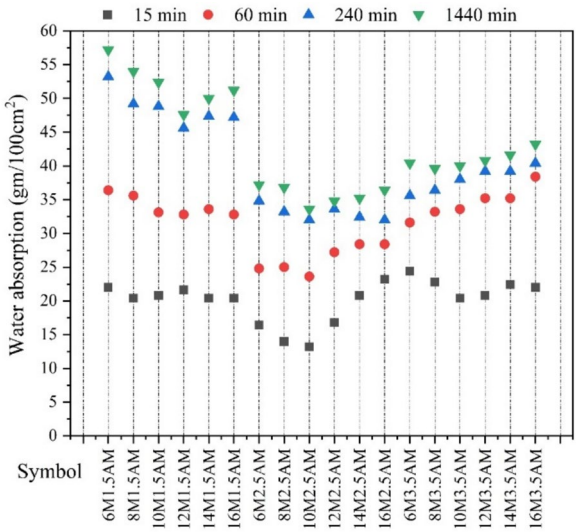

Fig. 9 Variation in water absorption due to capillary rise

solution results in a more viscous alkaline activator. This promotes faster and more extensive dissolution of aluminosilicate materials, leading to higher initial shrinkage. However, this rapid reaction can also result in more significant long-term shrinkage as the internal structure of the geopolymer continues to stabilize and densify over time. Conversely, mixes with lower AM ratios (1.5) and moderate molarity (6 M, 8 M) exhibit relatively stable shrinkage behavior. The lower sodium silicate content in these mixes results in a slower geopolymerization process, leading to more gradual water loss and reduced shrinkage. These mixes are potentially more suitable for applications where dimensional stability is crucial. While higher AM ratio mixes exhibit greater shrinkage, they may offer other benefits such as improved workability or strength, which should be weighed against their shrinkage behavior in practical applications.

3.3 Sorptivity

The variations in water absorption caused by capillary rise tested according to ASTM C1403 (ASTM C, 1403 2000) are shown in Fig. 9 for different AM ratios. Samples reported different levels of water absorptions at various exposure durations. The maximum water absorption due to capillarity from the 1.5AM mixture group was reported by the 6M1.5AM mixture with a magnitude of 57.33 gm/100cm^2, whereas the lowest by the 12M1.5AM mixture with a magnitude of 47.6 gm/100cm^2 after 24 h of testing. The maximum water absorption due to capillarity from the 2.5AM mix group is obtained by the 6M2.5AM mixture with a magnitude of 37.24 gm/100cm^2, whereas the lowest by the 10M2.5AM mixture with a magnitude of 33.20 gm/100cm^2. The maximum water absorption due to capillarity from the AM3.5 mix group is obtained by the 16M3.5AM mixture with a magnitude of 43.24 gm/100cm^2, whereas the lowest by the 8M3.5AM mixture with a magnitude of 39.60 gm/100cm^2. Hence, it was observed that different molarity and AM ratio values create a multi-level of capillary voids which changes the water absorption rate. From the obtained result, it was further deducted that increasing the molarity of the NaOH solution and the AM ratio value increases the voids in the hardened mortar. The increases in the void with the increases in the AM ratio can be directly associated with the rise in the Na_2SiO_3 content as 16 M NaOH-based solutions reported lower water absorptions due to capillarity till 2.5AM ratio mixture. In contrast, for AM3.5 ratio mixtures, the highest water absorption is reported by the 16 M NaOH-based mixture. The Na_2SiO_3 solution has a higher density and cohesiveness than the NaOH solution; hence, the abundance of Na_2SiO_3 creates voids within the mixture, and the extra quantity may increase the voids by forming micro air bubbles in the fresh state which eventually converts into voids in the hardened state.

3.4 Tensile Bond Strength

Figure 10 presents the variation in the tensile bond strength for different molarity and AM ratios. The 2.5AM mixtures group obtained the highest tensile bond strength among the group, and 12 M mixtures reported slightly higher values than the 10 M mixtures throughout the testing phases. The second highest strength as obtained by the 3.5AM mixture group and the least by the 1.5AM mixture group. In comparison, it could be observed that almost all of the mixtures attained their

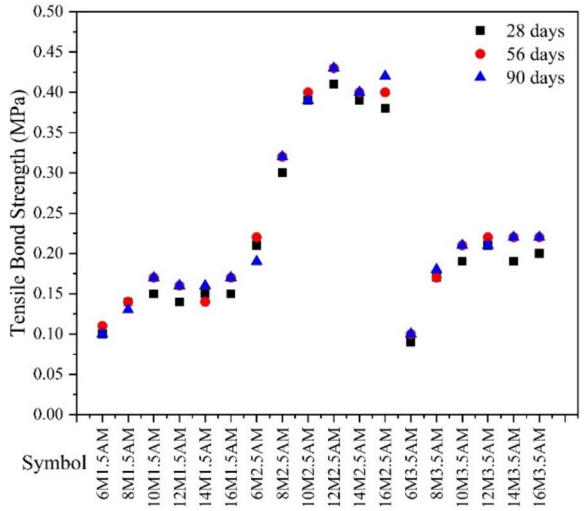

Fig. 10 Variation in tensile bond strength

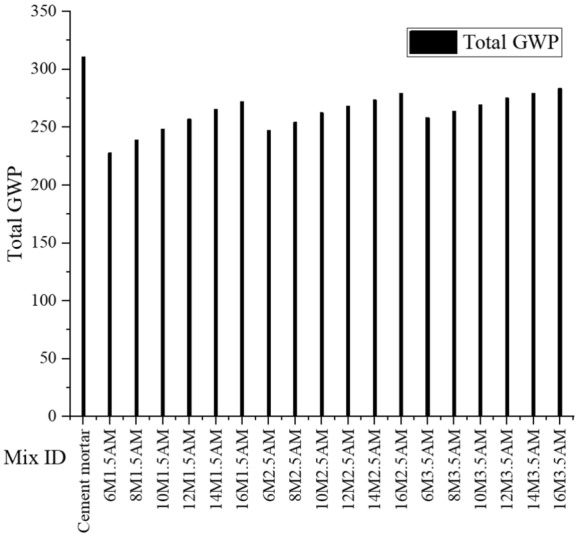

Fig. 11 Total GWP (kg CO_2-eq) for each batch of mortar

maximum tensile bond strength by 28 days, and beyond 28 days to 90 days, the increment in strength is very minimal. The ultimate tensile bond strength was achieved by the 12M2.5AM mixture of 0.41 MPa at 28 days and 0.43 MPa at 56 and 90 days. The least tensile bond strength was attained by 6M1.5AM and 6M3.5AM mixtures of around 0.09 to 0.11 MPa, irrespective of the curing age. From the output, it is evident that the long-term strength increments for 100% WCC powder-based samples are negligible.

3.5 Life Cycle Assessment and Impact Categories

The total GWP for 1 m^3 of the produced mortar with the reference cement mortar is presented in Fig. 11. It can be observed that geopolymer mortar made of WCC has less GWP impact on the environment. The reason behind this high GWP contribution by cement is the huge energy consumption during cement manufacturing from clinkers (Prakasan et al., 2020). Figure 12 presents the total GWP for each material of the produced mortar for one kg of utilized material. Therefore, from Fig. 12, it is identified that the alkalis are the constituents that are responsible for the maximum GWP contribution for geopolymer mortar. In contrast, data suggest that cement has a higher GWP impact than the sodium silicate (Na_2SiO_3) of 37% solid constituents, mostly used globally and also used in this study. Figure 13 presents the additional GWP impact due to heat curing of the samples at different curing temperatures for 24 h. From the presented graph, it is observed that increasing the curing temperature increases the amount of CO_2 emission into the environment. Figure 14 presents the relative compressive strength to the GWP index. Other than the 6M1.5AM and 6M3.5AM mixture, all other 100% WCC powder-based mixtures reported an average 30% reduction in GWP in comparison with the cement mortar.

Acidification potential (AP) is measured as the rise in precipitation pH induced by the washout of air pollutants, mostly SO_2, NH_3, and NO_x, in rivers/streams and soil. The total AP for 1 m^3 of the produced mortar specimens is presented in Fig. 15. It is observed that all the geopolymer mortars reported lesser value than the conventional cement mortar, which is a clear identification that geopolymers have less potential to release H^+ ions into the environment. But for the geopolymers, the total AP value rises with the increase

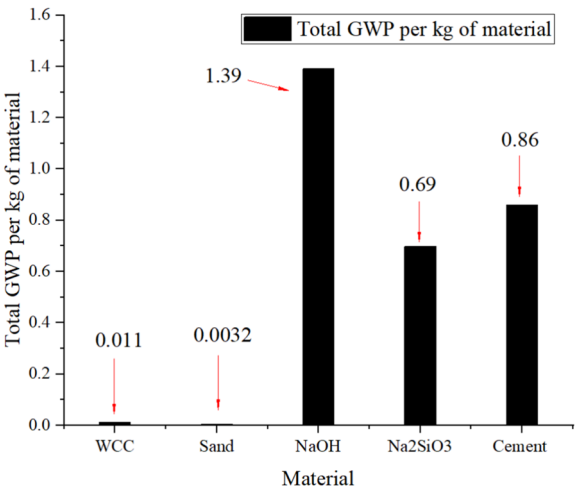

Fig. 12 Total GWP (kg CO_2-eq per kg) for per kg of material utilized

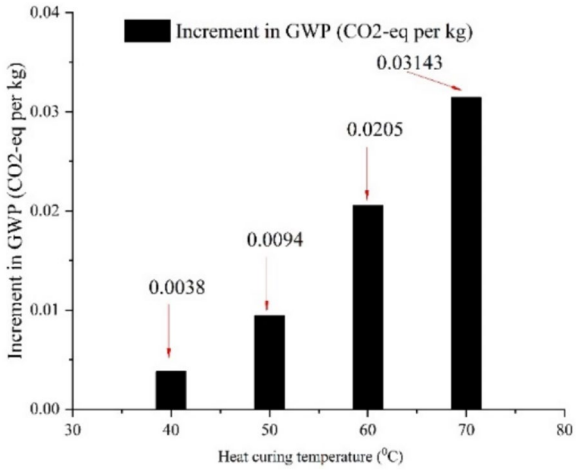

Fig. 13 Increment in GWP (CO_2-eq per kg) for heat curing

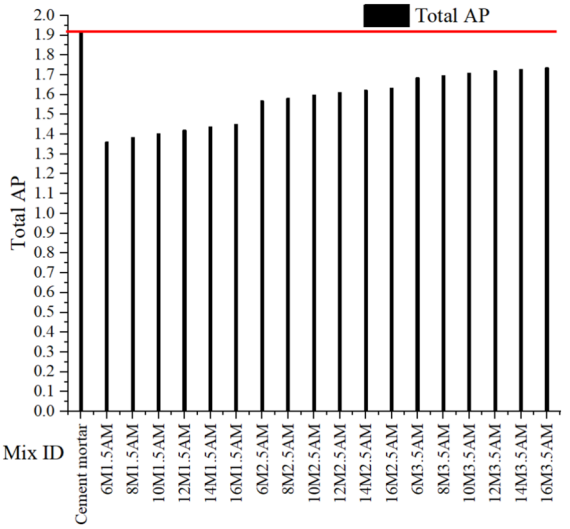

Fig. 15 Total AP (kg SO_2-eq) for each batch of mortar

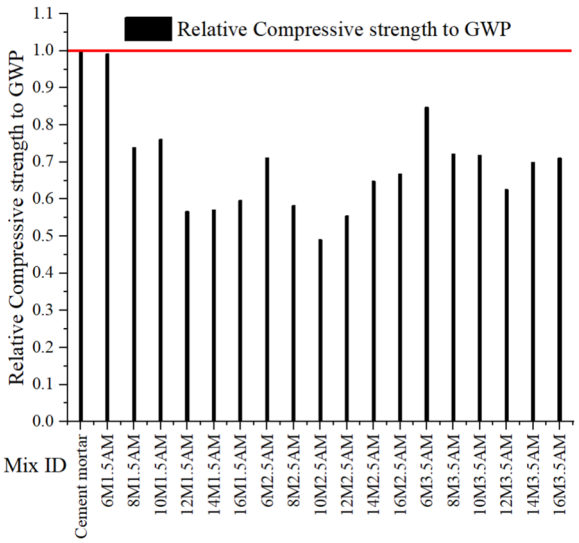

Fig. 14 Relative compressive strength to GWP index

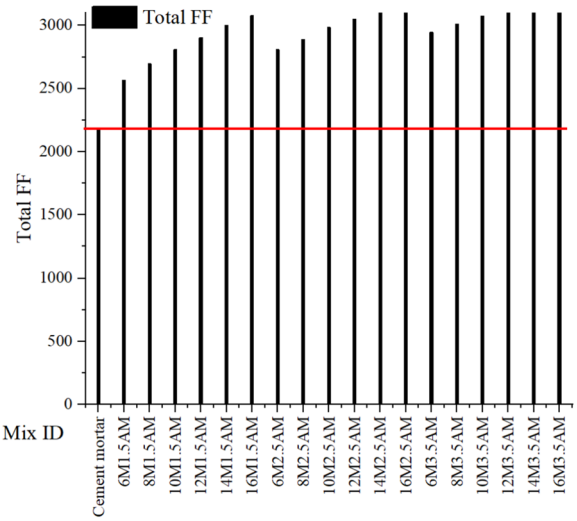

Fig. 16 Total FF (MJ per kg) for each batch of mortar

in the alkali content. Hence a lower alkali content will be a potential step for reducing the AP impact of geopolymers.

Finally, the total fossil fuel (MJ per kg) for each mortar batch presented in Fig. 16 clearly demonstrates that out of the three indicators, viz., GWP, AP, and FF, geopolymers reported higher values for the FF depletion category, which is majorly because of the utilization of sodium hydroxide in geopolymers. Sodium hydroxide has the highest fossil fuel consumption during its production stage, and the same can be observed from Fig. 16 that with the increment in the molarity of the mixtures, the FF depletion value increases.

3.6 Economical Assessment Through Cost–Benefit Analysis (CBA)

To perform the CBA, the cost of attainment of per unit MPa compressive strength for a traditional 1:3 cement mortar is considered as a reference. Hence, the relative compressive strength to cost index for the traditional cement mortar is taken as a magnitude of one. Thereafter whatever the cost incurred per unit MPa compressive strength attainment for different geopolymer mortars at different curing conditions is being divided by the reference. Hence, any index value greater than one showcases a lower CBA, and vice versa.

The relative compressive strength to cost indices for all the mix combinations cured at 30, 40, 50, 60 and 70 ℃ temperature is presented in Fig. 17. A combined analysis of these figures shows that with the increment in the curing temperature, more geopolymer samples reported higher cost-to-benefit value than the traditional cement mortar. It is noteworthy that, though heat curing incurs an extra cost on the overall process, it is beneficial by attaining better compressive strength in terms of cost incurred for production. However, further analysis of Fig. 17f shows that all the geopolymer samples, except 6M1.5AM, have a lower GWP for the developed compressive strength. This outcome from the geopolymer mortar is a sustainable approach in reducing the addition of CO_2 into the environment with comparable or better compressive strength attainment than conventional cement mortar.

3.6.1 Consolidated Index (ECM)

The consolidated index, depicted as ECM, is the combined index of the environmental, mechanical, and economical parameters. The ECM index is calculated using Eq. 3:

$$\mathrm{ECM} = \frac{\text{Mechanical index}}{\text{EnvScore} + \text{cost}}. \tag{3}$$

While calculating ECM, EnvScore and cost index are given equal weightage.

Figure 18 illustrates the relative ECM score for each mortar mixture. From the ECM index it could be observed that the geopolymer mortar mixtures have a better ECM index than the cement mortar. Among the geopolymers, 10M2.5AM mixture reported the maximum value. This result clearly signifies that the geopolymer mortar prepared by utilizing WCC has a better output combining mechanical, economical, and environmental parameters.

3.7 Optimization Through Central Composite Design

3.7.1 ANOVA

This study evaluates the effects of molarity, alkaline ratio, and their interactions on the properties of geopolymer mortar using waste concrete powder. The responses examined include compressive strength, shrinkage, tensile bond, sorptivity, and GWP. The significance of these factors was determined using ANOVA, along with their percentage contribution to the total variability. The significance levels for each factor were calculated based on their p-values. If the p-value was less than 0.05, the factor was considered significant; otherwise, it was considered not significant. Additionally, the percentage contribution of each factor was calculated by dividing the sum of squares for that factor by the total sum of squares and multiplying by 100.

Table 8 presents comprehensive data for the factors involved and their responses. The ANOVA results indicate that the molarity ($p=0.002$) and the interaction between molarity and alkaline ratio ($p=0.0304$) significantly influence compressive strength, suggesting that both the concentration of the activating solution and the interaction between components are crucial for strength development. The alkaline ratio alone ($p=0.5755$) was not significant. Molarity contributed 53.22% to the variability in compressive strength, while the interaction contributed 18.99%. Shrinkage was significantly affected by molarity ($p=0.0049$), the interaction between molarity and alkaline ratio ($p=0.0257$), and the quadratic terms of molarity (A^2, $p=0.0013$) and alkaline ratio (B^2, $p<0.0001$). These results highlight the complexity of shrinkage behavior, emphasizing the importance of both the concentration and balance of the activating solutions in minimizing shrinkage. The quadratic term of the alkaline ratio had the highest contribution to shrinkage at 88.75%.

Tensile bond strength was significantly influenced by molarity ($p=0.0025$), and the quadratic terms of molarity (A^2, $p=0.0115$) and alkaline ratio (B^2, $p<0.0001$). The interaction between molarity and alkaline ratio was not significant ($p=0.2962$). This underscores the critical role of optimizing the concentrations of the activating solutions for enhancing bonding properties. The quadratic term of the alkaline ratio contributed the most to tensile bond strength, with 51.64%. Sorptivity, which measures water absorption capacity, was significantly affected by the alkaline ratio ($p<0.0001$), the interaction between molarity and alkaline ratio ($p=0.0051$), and the quadratic terms of both molarity (A^2, $p=0.0066$) and alkaline ratio (B^2, $p<0.0001$). Molarity alone was not significant ($p=0.2095$), indicating that reducing water absorption requires careful adjustment of the alkaline components and their concentrations. The quadratic term of the alkaline ratio had the highest contribution to sorptivity at 45.43%.

The GWP was significantly influenced by all factors: molarity ($p<0.0001$), alkaline ratio ($p<0.0001$), their interaction ($p<0.0001$), and their quadratic terms (A^2, $p=0.0038$ and B^2, $p=0.0008$). This demonstrates the potential for optimizing the mix design to minimize the environmental footprint while achieving desirable mechanical properties. Molarity contributed 66.66% to GWP, indicating its dominant influence on environmental impact.

Finally, the ANOVA results demonstrate that the properties of geopolymer mortar using waste concrete powder are significantly influenced by molarity, alkaline

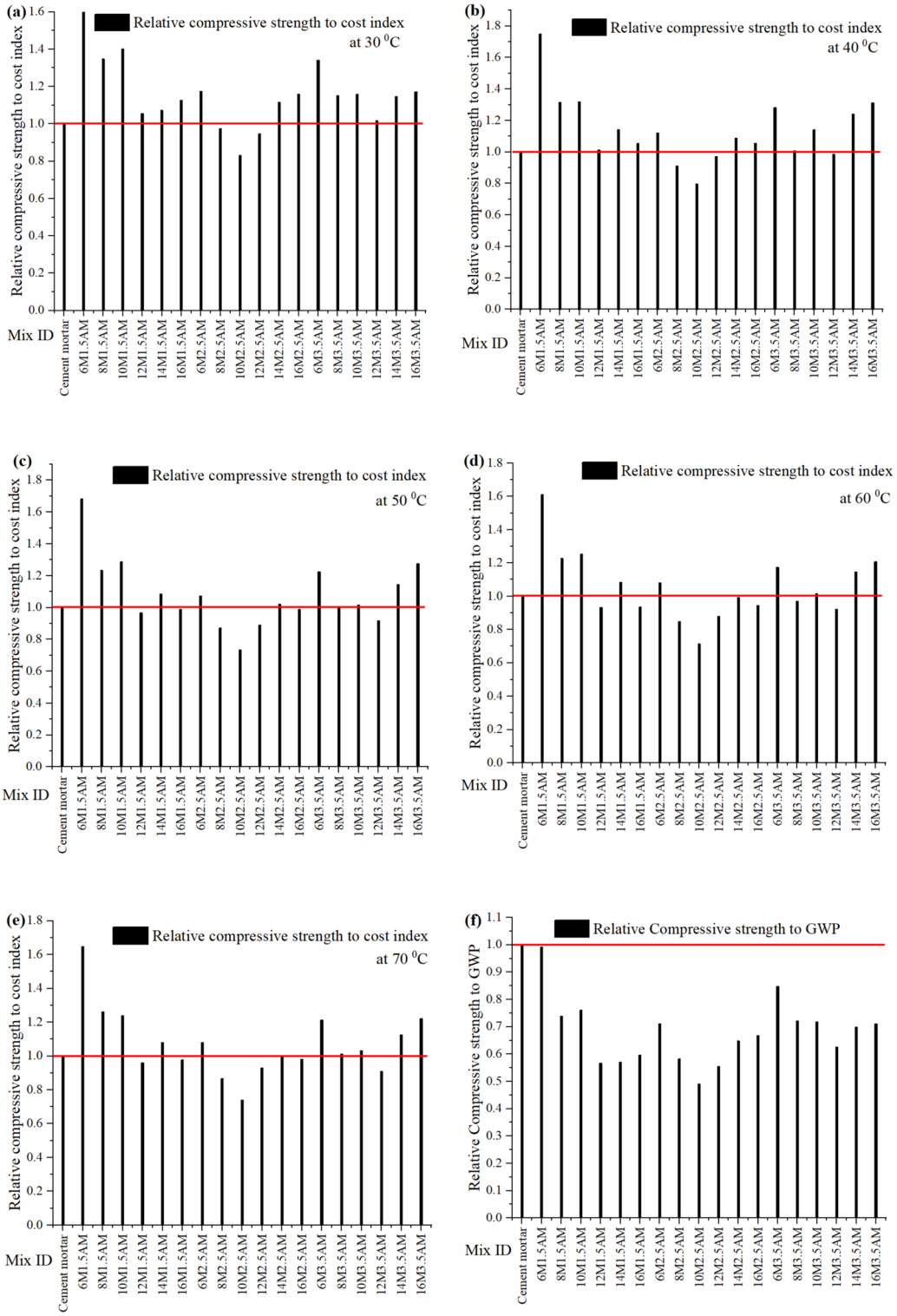

Fig. 17 Relative compressive strength to cost at multiple curing temperatures and GWP: **a** 30 ˚C, **b** 40 ˚C, **c** 50 ˚C, **d** 60 ˚C, **e** 70 ˚C and **f** GWP

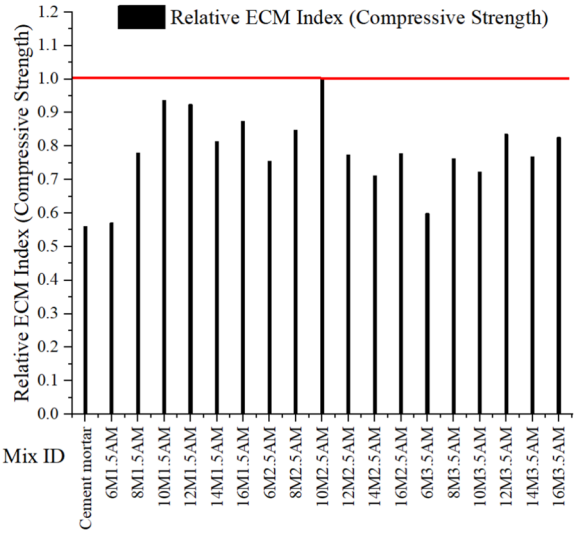

Fig. 18 Relative ECM index for 28-day compressive strength attainment by different mortar mixtures cured at controlled ambient temperature

ratio, and their interactions. The study emphasizes the importance of optimizing these factors to achieve both high performance and sustainability. Geopolymer mortars have the potential to address environmental and economic challenges in the construction industry, promoting greener construction practices and innovative material development. The percentage contributions of each factor highlight the most influential parameters for each response, guiding future optimization efforts. The calculation of significance levels based on p-values provides a robust method for identifying key factors impacting the properties of geopolymer mortar.

3.8 Statistical Fit Summary

The fit summary is presented in Table 9, which provides a comprehensive overview of the statistical metrics. The table highlights the significance of different models (Linear, 2FI, Quadratic, and Cubic) for each response variable based on their sequential p-values, lack of fit p-values, adjusted R^2, and predicted R^2 values.

For compressive strength, the linear model is significant with a sequential p-value of 0.0184, but it shows a poor fit with a negative adjusted R^2 value of −0.1678. The 2FI model is suggested based on a sequential p-value of 0.0304 and a lack of fit p-value of 0.6537, although it also shows a poor fit with an adjusted R^2 value of −0.6282. The quadratic and cubic models do not provide better fits, as indicated by their higher p-values and negative adjusted R^2 values, with the cubic model being aliased.

For sorptivity, neither the linear nor 2FI models are significant, with sequential p-values of 0.1969 and 0.5151, respectively, and negative adjusted R^2 values indicating poor fits. The quadratic model is suggested with a sequential p-value of < 0.0001, a high adjusted R^2 value of 0.8556, and a high predicted R^2 value of 0.9739, indicating a very good fit. The cubic model is aliased, showing a slightly lower adjusted R^2 of 0.5876.

For shrinkage, the linear and 2FI models are not significant, with sequential p-values of 0.5316 and 0.433, respectively, and negative adjusted R^2 values indicating poor fits. The quadratic model is suggested with a sequential *p*-value of < 0.0001 and an adjusted R^2 value of 0.4541, showing a better fit compared to the linear and 2FI models. The cubic model is aliased, with an adjusted R^2 value of 0.4298.

For tensile bond, the linear and 2FI models are not significant, with sequential p-values of 0.4197 and 0.8116, respectively, and negative adjusted R^2 values. The quadratic model is suggested, showing a sequential *p*-value of < 0.0001, an adjusted R^2 of 0.9473, and a predicted R^2 of 0.6825, indicating a good fit. The cubic model, although aliased, shows an even higher adjusted R^2 of 0.9762 but a negative predicted R^2, suggesting overfitting.

For GWP, all models (Linear, 2FI, quadratic, and cubic) are significant with very low sequential *p*-values (all less than 0.001). The linear model has an adjusted R^2 of 0.8378, while the 2FI model improves this to 0.8871. The quadratic model is suggested, with the highest adjusted R^2 of 0.9827 and a predicted R^2 of 0.9974, indicating an excellent fit. The cubic model, while aliased, shows a slightly higher adjusted R^2 of 0.9881.

The analysis reveals that the quadratic model is generally the best fit for most responses, particularly sorptivity, shrinkage, tensile bond, and GWP, as indicated by their high adjusted and predicted R^2 values. The significance of the models is determined by the sequential p-values, with values less than 0.05 indicating significant models. The presence of aliased models suggests potential issues with model complexity and overfitting. Overall, the study emphasizes the importance of selecting appropriate models to accurately capture the behavior of geopolymer mortar properties, thereby facilitating the optimization of mix designs for enhanced performance and sustainability.

Compressive strength is positively influenced by both molarity and alkaline ratio, though their combined high levels slightly reduce the strength. Sorptivity decreases with higher molarity and alkaline ratio, beneficial for durability, and shows a non-linear relationship requiring careful balancing of factors. Tensile bond strength improves with higher molarity and alkaline ratio, with minimal interaction effects, but shows diminishing returns at higher levels. GWP increases with both factors but can be minimized by optimizing their levels, considering the slight reduction by interaction and quadratic terms. Shrinkage increases

Table 8 ANOVA of factor and response

Factor	Response	Sum of squares	df	Mean square	F-value	p-value	Significance	% Contribution
Molarity	Compressive strength	44.21	1	44.21	18.44	0.002	Significant	53.22%
	Shrinkage	1.59×10^{-6}	1	1.59×10^{-6}	16.35	0.0049	Significant	14.93%
	Tensile bond	0.0181	1	0.0181	21.09	0.0025	Significant	9.23%
	Sorptivity	2.67	1	2.67	1.91	0.2095	Not significant	0.42%
	GWP	1719.75	1	1719.75	3022.43	< 0.0001	Significant	66.66%
Alkaline mix ratio	Compressive strength	0.8091	1	0.8091	0.3375	0.5755	Not significant	0.97%
	Shrinkage	8.95×10^{-8}	1	8.95×10^{-8}	0.9189	0.3697	Not significant	0.08%
	Tensile bond	0.0018	1	0.0018	2.06	0.1945	Not significant	0.92%
	Sorptivity	175.34	1	175.34	125.55	< 0.0001	Significant	27.35%
	GWP	646.24	1	646.24	1135.75	< 0.0001	Significant	25.05%
Molarity x alkaline ratio	Compressive strength	15.79	1	15.79	6.59	0.0304	Significant	18.99%
	Shrinkage	7.76×10^{-7}	1	7.76×10^{-7}	7.97	0.0257	Significant	7.29%
	Tensile bond	0.0011	1	0.0011	1.27	0.2962	Not significant	0.56%
	Sorptivity	22.48	1	22.48	16.1	0.0051	Significant	3.51%
	GWP	106.82	1	106.82	187.73	< 0.0001	Significant	4.14%
A^2	Compressive strength	–	–	–	–	–	–	–
	Sorptivity	20.3	1	20.3	14.53	0.0066	Significant	3.17%
	Shrinkage	2.60×10^{-6}	1	2.60×10^{-6}	26.67	0.0013	Significant	24.43%
	Tensile bond	0.0099	1	0.0099	11.56	0.0115	Significant	5.05%
	GWP	10.27	1	10.27	18.05	0.0038	Significant	0.40%
B^2	Compressive strength	–	–	–	–	–	–	–
	Sorptivity	291.25	1	291.25	208.54	< 0.0001	Significant	45.43%
	Shrinkage	9.45×10^{-6}	1	9.45×10^{-6}	97.07	< 0.0001	Significant	88.75%
	Tensile bond	0.1013	1	0.1013	117.78	< 0.0001	Significant	51.64%
	GWP	17.71	1	17.71	31.12	0.0008	Significant	0.69%
Model	Compressive strength	61.5	3	20.5	8.55	0.0053	Significant	74.05%
	Shrinkage	0	5	2.39×10^{-6}	24.58	0.0003	Significant	0%
	Tensile bond	0.1901	5	0.038	44.18	< 0.0001	Significant	96.94%
	Sorptivity	631.38	5	126.28	90.42	< 0.0001	Significant	98.47%
	GWP	2580.8	5	516.16	907.14	< 0.0001	Significant	100%
Residual	Compressive strength	21.58	9	2.4				25.95%
	Shrinkage	6.81×10^{-7}	7	9.73×10^{-8}				0.62%
	Tensile bond	0.006	7	0.0009				3.06%
	Sorptivity	9.78	7	1.4				1.53%
	GWP	3.98	7	0.569				0.15%
Lack of fit	Compressive strength	21.58	5	4.32				
	Shrinkage	6.81×10^{-7}	3	2.27×10^{-7}				
	Tensile bond	0.0059	3	0.002	65.59	0.0007	Significant	
	Sorptivity	9.78	3	3.26				
	GWP	3.98	3	1.33				
Pure error	Compressive strength	0	4	0				
	Shrinkage	0	4	0				
	Tensile bond	0.0001	4	0				
	Sorptivity	0	4	0				
	GWP	0	4	0				
Cor total	Compressive strength	83.08	12					
	Shrinkage	0	12					
	Tensile bond	0.1961	12					
	Sorptivity	641.16	12					

Table 8 (continued)

Factor	Response	Sum of squares	df	Mean square	F-value	p-value	Significance	% Contribution
	GWP	2580.8	12					

Table 9 Statistical fit summary of factors responses

Response	Source	Sequential *p*-value	Lack of fit *p*-value	Adjusted R^2	Predicted R^2	Notes
Compressive strength	Linear	0.02	0.46	−0.17		
	2FI	0.03	0.65	−0.63	Suggested	
	Quadratic	0.12	0.76	−0.33		
	Cubic	0.27	0.80	−10.02		Aliased
Sorptivity	Linear	0.20	0.13	−0.53		
	2FI	0.52	0.08	−2.46		
	Quadratic	< 0.0001	0.97	0.86	Suggested	
	Cubic	0.02	0.99	0.59		Aliased
Shrinkage	Linear	0.53	−0.06	−0.62		
	2FI	0.43	−0.09	−0.84		
	Quadratic	< 0.0001	0.91	0.45	Suggested	
	Cubic	0.00	0.99	0.43		Aliased
Tensile bond	Linear	0.42	< 0.0001	−0.01	−0.5805	
	2FI	0.81	< 0.0001	−0.11	−2.278	
	Quadratic	< 0.0001	0.00	0.95	0.6825	Suggested
	Cubic	0.06	0.00	0.98	−0.2333	Aliased
Global warming potential (GWP)	Linear	0.00	0.93	0.84		
	2FI	0.00	0.98	0.89		
	Quadratic	0.00	1.00	0.98	Suggested	
	Cubic	0.00	1.00	0.99		Aliased

significantly with higher molarity and alkaline ratio, necessitating careful control to maintain dimensional stability.

These equations offer predictive tools for optimizing mix designs to achieve desired mechanical properties while minimizing environmental impact. The non-linear relationships highlight the complexity and the need for a balanced approach to material formulation.

$$\text{Compressive strength} = (-0.7475 + 1.5240 \times \text{molarity} + 3.9737 \times \text{AM} - 0.3947 \times (\text{molarity} \times \text{AM}) \tag{4}$$

$$\text{Sorptivity} = (140.5241 - 3.8186 \times \text{molarity} - 61.9501 \times \text{alkaline ratio} + 0.4711 \times (\text{molarity} \times \text{AM}) + 0.1140 \times (\text{molarity2}) + 10.2690 \times (\text{AM2})) \tag{5}$$

$$\text{Tensile bond} = (-1.1970 + 0.0583 \times \text{molarity} + 0.9388 \times \text{AM} + 0.0033 \times (\text{molarity} \times \text{AM}) - 0.0025 \times (\text{molarity2}) - 0.1916 \times (\text{AM2})) \tag{6}$$

$$\text{GWP} = (147.6705 + 7.7367 \times \text{molarity} + 34.3664 \times \text{AM} - 1.0267 \times (\text{molarity} \times \text{AM}) - 0.0811 \times (\text{molarity2}) - 2.5321 \times (\text{AM2}) \tag{7}$$

$$\text{Drying shrinkage} = (1.59 \times 10-6 \times \text{molarity} + 8.94 \times 10-8 \times \text{alkaline ratio} + 7.75 \times 10-7 \times (\text{molarity} \times \text{AM}) + 2.59 \times 10-6 \times (\text{molarity2}) + 9.45 \times 10-6 \times (\text{AM2})). \tag{8}$$

3.8.1 Interaction Plots

The interaction plots illustrate the combined effects of the factors and highlight significant interactions. Figure 19 presents the interactive plots for different responses.

The interaction plot for compressive strength shows that both molarity and AM ratio positively influence compressive strength. As molarity increases, compressive strength increases significantly, with a more pronounced effect when the AM ratio is at its higher level

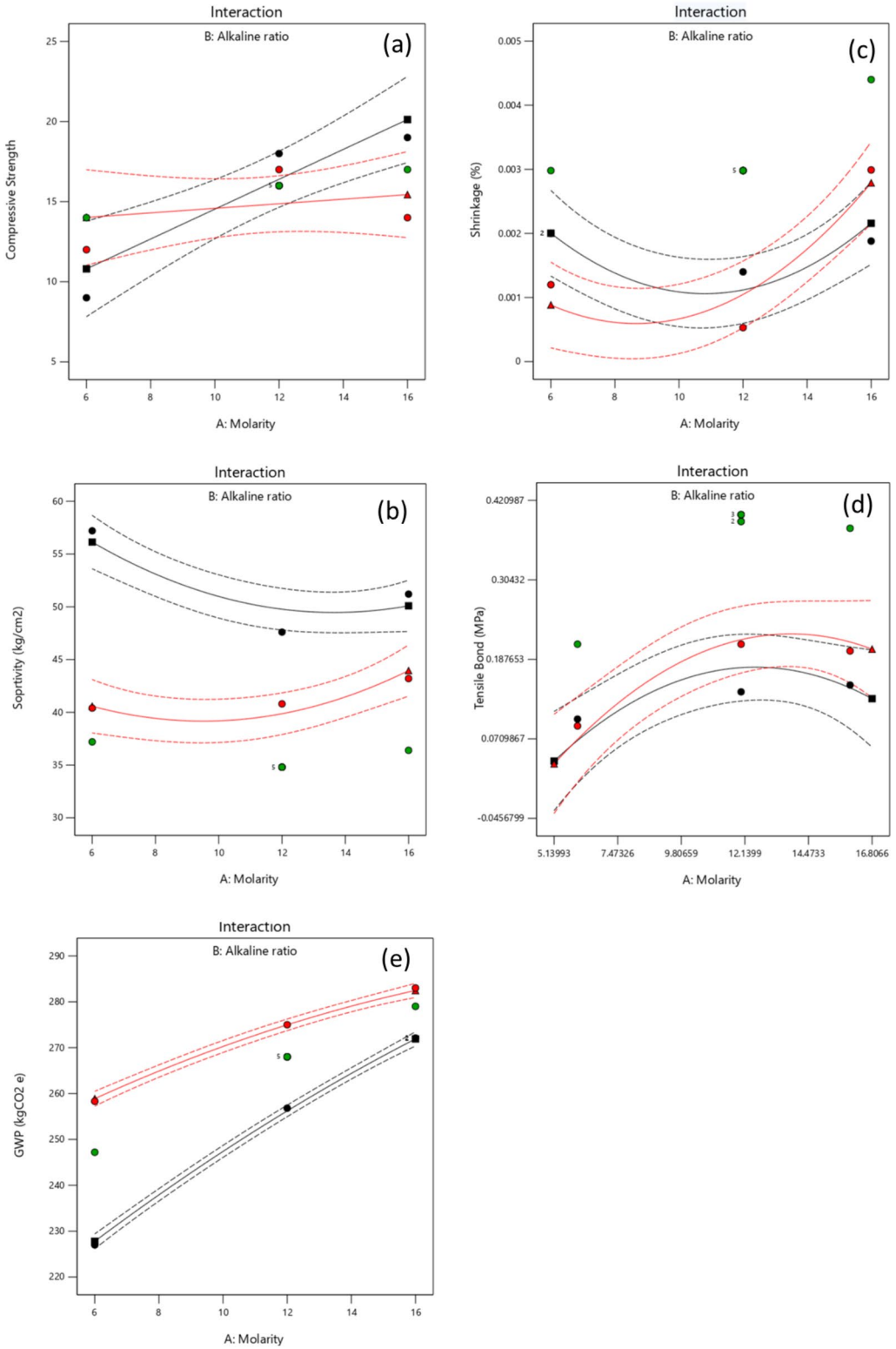

Fig. 19 Interactive plots for different responses. **a** Compressive strength, **b** sorptivity, **c** shrinkage, **d** tensile bond, **e** global warming potential

(3.5). The interaction between these two factors indicates that optimizing both parameters simultaneously can achieve higher compressive strength.

For sorptivity, the plot reveals a significant interaction between molarity and AM ratio. At a lower AM ratio (1.5), sorptivity decreases slightly with increasing molarity. However, at a higher AM ratio (3.5), sorptivity decreases more sharply with increasing molarity. This suggests that a higher AM ratio is more effective in reducing water absorption, especially when combined with higher molarity levels.

The shrinkage plot demonstrates a complex interaction between molarity and AM ratio. Shrinkage decreases slightly with increasing molarity at lower AM ratios but increases significantly at higher AM ratios. This indicates that while increasing molarity can help reduce shrinkage at low AM ratios, it can lead to higher shrinkage at elevated AM ratios. Thus, careful optimization of both parameters is necessary to minimize shrinkage.

The interaction plot for tensile bond strength indicates that both molarity and AM ratio positively influence bond strength, with the most substantial effect observed when both factors are at higher levels. The plot shows that tensile bond strength increases with molarity up to an optimal point, after which it starts to decline. This suggests that there is an optimal range for molarity and AM ratio to achieve maximum tensile bond strength.

For GWP, the interaction plot shows that increasing both molarity and AM ratio leads to a higher environmental impact. The plot indicates a linear increase in GWP with both factors, with a steeper slope observed for AM ratio. This highlights the need to balance the optimization of mechanical properties with the environmental impact, aiming to minimize GWP while achieving desired performance.

3.8.2 Surface Plots

The surface plots (Fig. 20) provide a three-dimensional visualization of the relationship between the independent variables (molarity and AM ratio) and the responses: compressive strength, sorptivity, shrinkage, tensile bond, and GWP. The surface plot for compressive strength shows a positive correlation with both molarity and AM ratio. As both parameters increase, the compressive strength also increases, with the highest values observed at higher levels of molarity (up to 16) and AM ratio (up to 3.5). This indicates that a combination of higher molarity and AM ratio leads to stronger geopolymer mortar.

The sorptivity plot exhibits a non-linear relationship with molarity and AM ratio. The lowest sorptivity values are achieved at intermediate levels of molarity (around 10) and AM ratio (around 2.5). Increasing either parameter beyond these levels results in increased sorptivity, indicating an optimal range for minimizing water absorption, which is critical for enhancing durability.

For shrinkage, the surface plot shows complex interactions between molarity and AM ratio. The lowest shrinkage occurs at lower molarity (around 6) and higher AM ratio (up to 3.5). As molarity increases, shrinkage tends to increase, particularly at lower AM ratios. This highlights the importance of optimizing both parameters to control shrinkage and maintain dimensional stability.

The surface plot for tensile bond strength indicates that both molarity and AM ratio contribute positively to the bond strength, with a peak observed at intermediate values of molarity (around 10) and AM ratio (around 2.5). Beyond these levels, the tensile bond strength starts to decline, suggesting an optimal range for achieving maximum bond strength.

GWP surface plot shows that increasing both molarity and AM ratio leads to higher environmental impact. The lowest GWP values are observed at lower levels of both parameters (molarity around 6 and AM ratio around 1.5). This indicates that while optimizing for mechanical properties, it is also essential to consider the environmental impact and find a balance that minimizes GWP.

3.8.3 Analysis of Diagnostic Study of Response

The predicted values closely align with the observed values for all responses, demonstrating the accuracy and reliability of the predictive models. The narrow 95% confidence intervals for the means indicate high precision in the predictions, while the broader 95% tolerance intervals for 99% of the population reflect the natural variability within the material properties. This analysis confirms the robustness of the models in predicting the behavior of geopolymer mortars, supporting their application in optimizing material properties for practical use.

3.8.3.1 Residuals and Predicted Values Residuals, which are the differences between actual and predicted values, serve as a primary indicator of the model's accuracy. Across all responses, smaller residuals denote more accurate predictions. For instance, in the compressive strength report, Run Order 1 had a notable residual of −2.0149, indicating the model overestimated the actual value. Similarly, in the sorptivity report, Run Order 2 had a significant negative residual of −2.1733, while Run Order 7 had a positive residual of 1.0647. The shrinkage report highlighted Run Order 1 with a residual of 0.0003166, and the tensile bond report showed Run Order 7 with a positive residual of 0.0313. In the GWP report, Run Order 7 stood out with a negative residual of −0.7835. These residuals indicate deviations between observed and predicted values, which, if large, can lead to inaccuracies in the model's

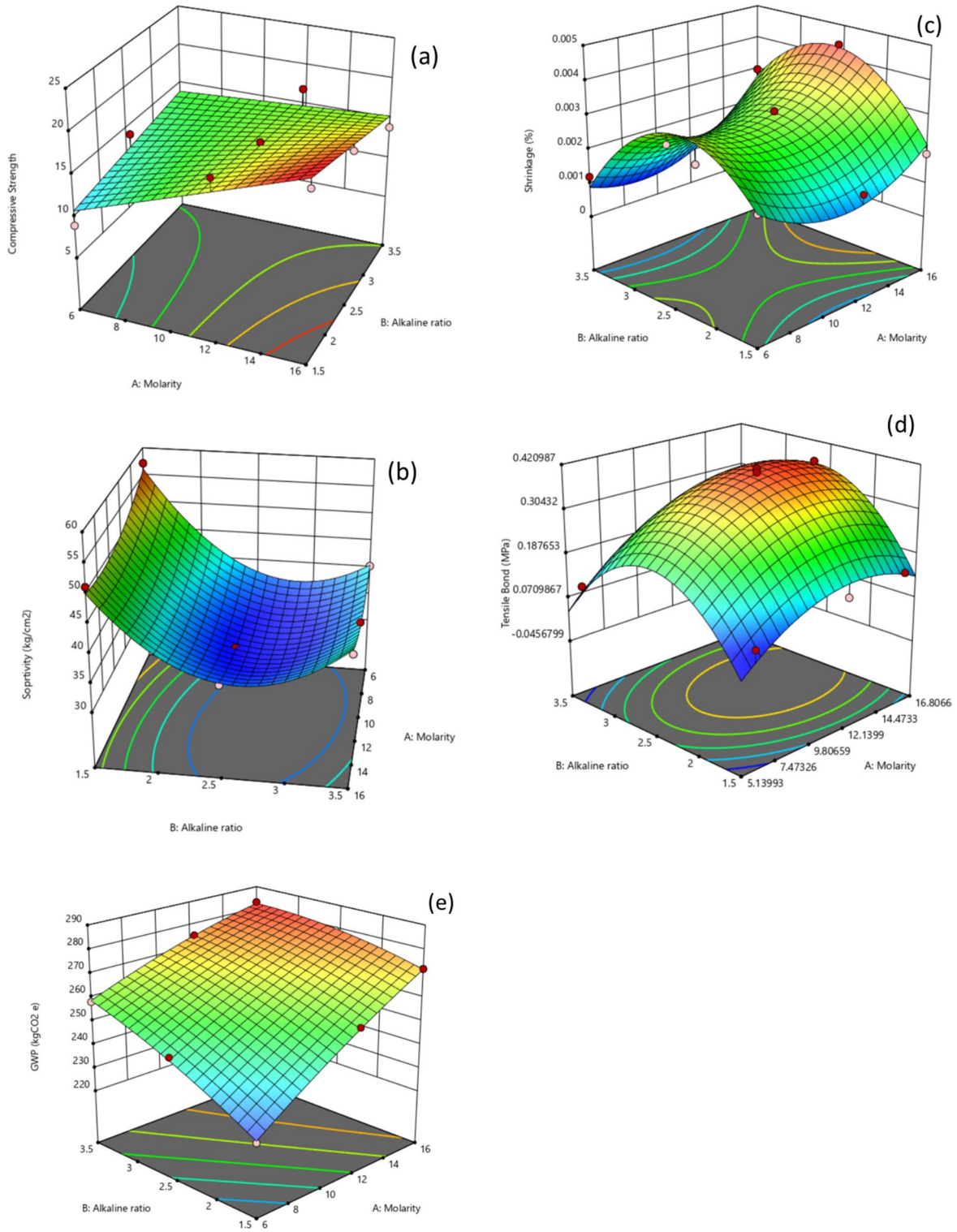

Fig. 20 Surface plots for responses. **a** Compressive strength, **b** sorptivity, **c** shrinkage, **d** tensile bond, **e** global warming potential

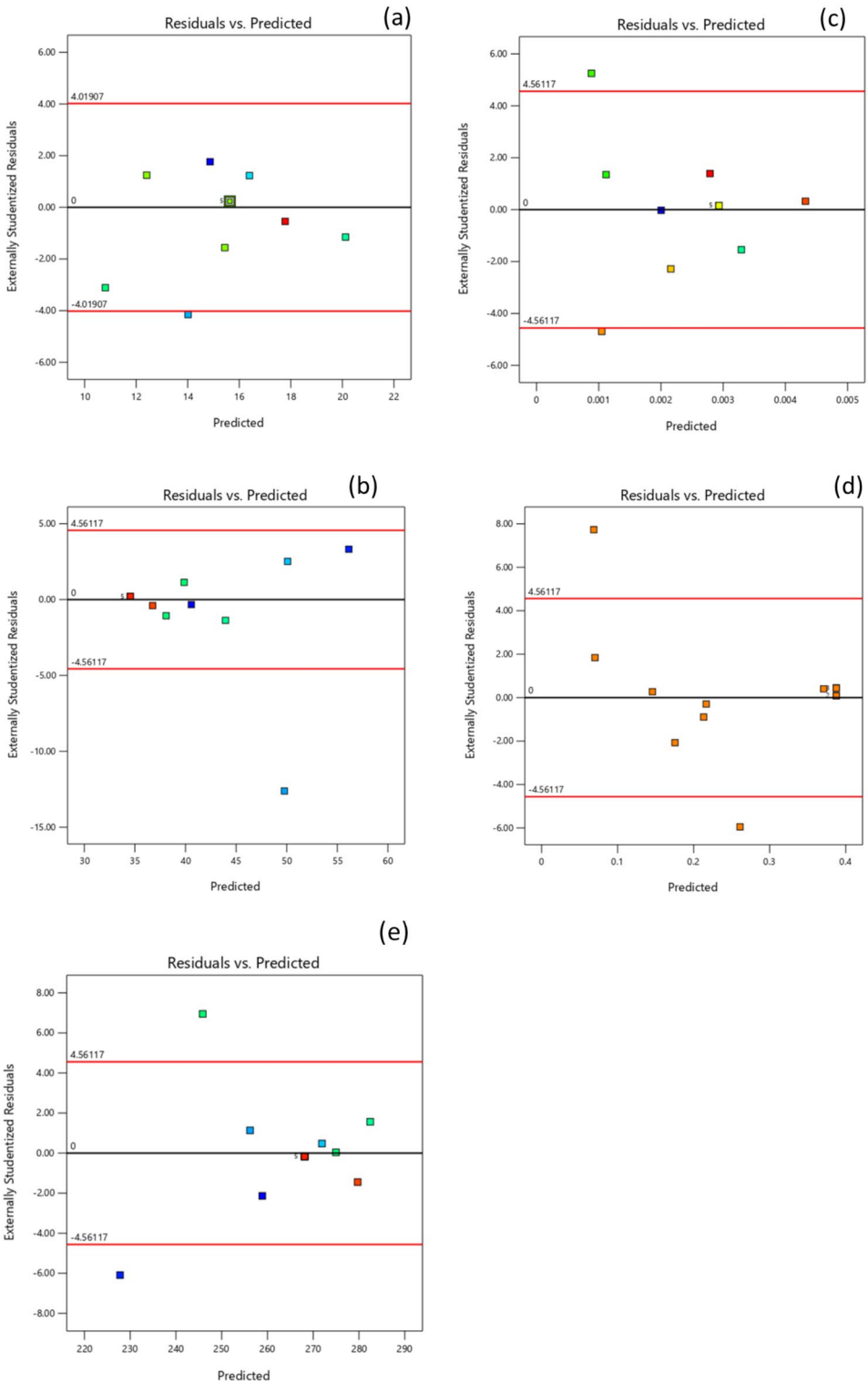

Fig. 21 Residual vs predicted values of the responses. **a** Compressive strength, **b** sorptivity, **c** shrinkage, **d** tensile bond, **e** global warming potential

predictive capabilities. Figure 21 shows the residual v/s predicted values for all the responses.

3.8.3.2 Leverage and Influence Leverage values measure each observation's impact on the model's fit. High leverage values indicate observations with greater influence. For compressive strength, Run Orders 1 and 7 had high leverage values of 0.8209. In sorptivity, Run Orders 1 and 7 again demonstrated high leverage, similar to the shrinkage report where Run Orders 1 and 7 were also influential. The tensile bond report showed high leverage for Run Orders 1 and 7, while the GWP report highlighted Run Orders 1 and 7 for their significant leverage values. High leverage points can disproportionately influence the model's parameters, leading to biased estimations and potentially reducing the model's overall accuracy.

3.8.3.3 Internally and Externally Studentized Residuals Internally studentized residuals account for dataset variation, while externally studentized residuals help identify outliers after a point is removed from the model. Significant outliers were found in compressive strength (Run Order 1 with −4.1511), sorptivity (Run Order 2 with −12.6144 and Run Order 7 with 3.3204), shrinkage (Run Orders 1 and 9 with −4.6912), tensile bond (Run Orders 7 with 7.7296 and 13 with −5.9486), and GWP (Run Order 7 with −6.0899 and Run Order 13 with 6.9518). These outliers can distort the model's predictions, leading to reduced accuracy and reliability, as the model may not generalize well to new data.

3.8.3.4 Cook's Distance and DFFITS Cook's distance and DFFITS quantify each observation's influence on the model's parameters and fitted values. High Cook's distance and DFFITS values indicate observations with a significant impact. In compressive strength, Run Orders 1 and 7 had notable Cook's distance and DFFITS values. Sorptivity showed high influence for Run Orders 2 and 7. Shrinkage highlighted Run Orders 1 and 9, while tensile bond pointed to Run Orders 7 and 13. The GWP report underscored Run Orders 7 and 13 as having substantial influence. These metrics help identify observations that, if removed, would significantly alter the model's predictions, indicating their potential to skew the model if left unaddressed.

3.8.4 Multi-response Desirability Analysis

Multi-response desirability analysis was carried out for all responses. Equal weightage and importance were given to all the response. Table 10 shows the weightage, importance and optimization considered for optimization the optimal levels for WCC-based geopolymer mortar.

Table 10 Importance factor, weightage and optimization conditions for all responses

Response	Weightage	Importance factor	Optimization condition
Compressive strength	1	+ + +	Maximize
Sorptivity	1	+ + + +	Minimize
Shrinkage	1	+ + +	Minimize
Tensile bond	1	+ + +	Maximize
GWP	1	+ + +	Minimize

In the desirability plot (Fig. 22), the green area represents the highest desirability, with a peak desirability score of around 0.6 located at a molarity of approximately 11.2 and an AM ratio of about 2.5. This area signifies the optimal conditions for achieving the best balance across all responses. For compressive strength, the plot shows an increase in strength with higher levels of molarity and AM ratio, moving from green (lower strength) to red (higher strength). The highest compressive strength is observed at higher molarity (around 16) and AM ratio (around 3.5).

The sorptivity plot indicates a lower water absorption capacity with decreasing values, moving from blue (high sorptivity) to green (low sorptivity). The optimal condition for minimizing sorptivity aligns with the region of highest desirability, at a molarity of around 11.2 and an AM ratio of about 2.5. The shrinkage plot shows minimal shrinkage in the blue areas (low shrinkage) and higher shrinkage in the green to yellow areas. The lowest shrinkage values are observed at lower molarity (around 8) and a higher AM ratio (around 3.5).

For tensile bond strength, the plot shows increasing bond strength with higher levels of both molarity and AM ratio, moving from green (lower strength) to red (higher strength). The highest tensile bond strength is observed at a molarity of approximately 11.2 and an AM ratio of about 2.5, which is consistent with the optimal desirability region. The GWP plot, which shows the environmental impact, has lower values indicated by green and higher values by red. The lowest GWP is observed at a molarity of around 8 and an AM ratio of about 1.5, which does not coincide with the region of highest desirability, indicating a trade-off between minimizing environmental impact and optimizing other performance properties.

Overall, the desirability analysis helps identify the optimal conditions for molarity and AM ratio to achieve a balance across multiple responses. The region around

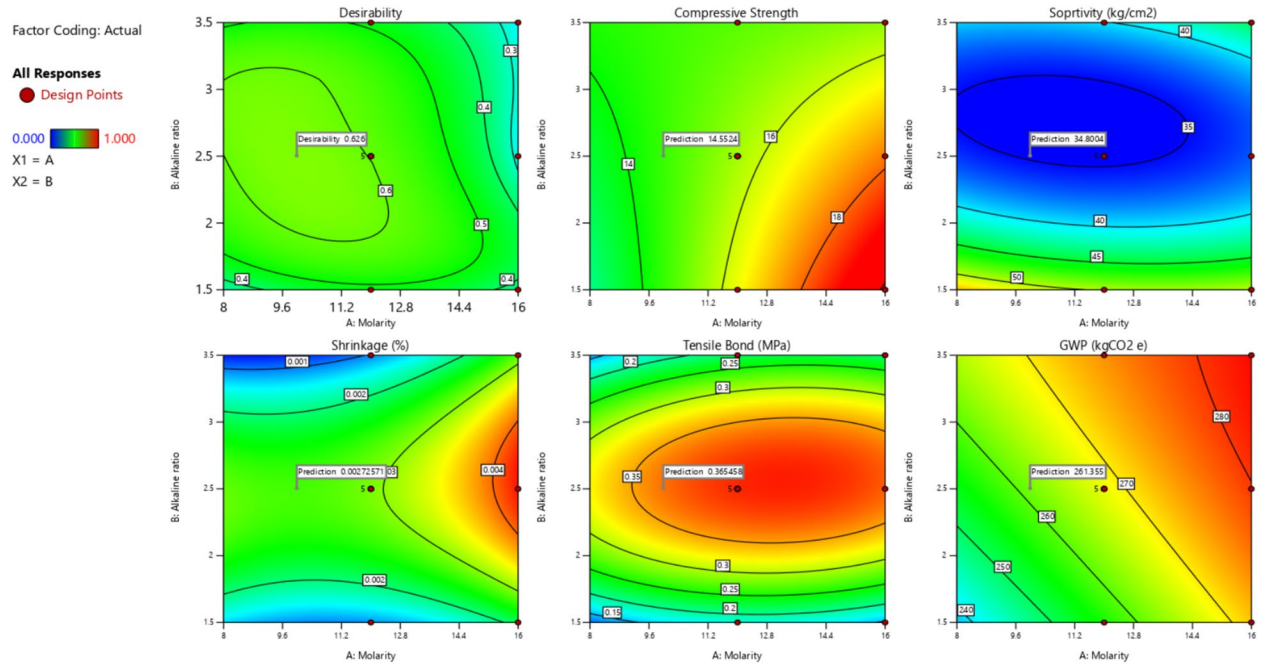

Fig. 22 Multi-response desirability plot

a molarity of 11.2 and an AM ratio of 2.5 is highlighted as the most desirable for achieving high compressive strength, low sorptivity, and high tensile bond strength while managing shrinkage and GWP. This analysis aids in the formulation of geopolymer mortar with optimized properties for practical applications.

The perturbation plots (Fig. 23) reveal the sensitivity of each response to changes in molarity and AM ratio. Molarity significantly influences compressive strength,

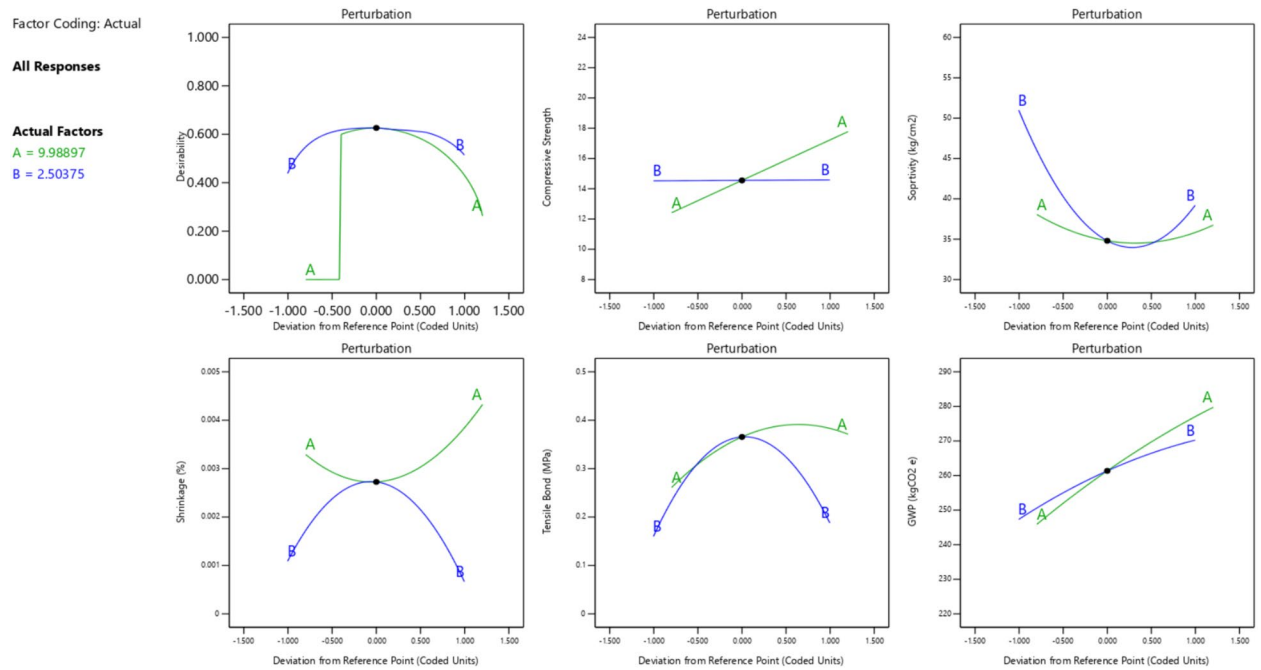

Fig. 23 Sensitivity analysis by perturbation plot

sorptivity, and shrinkage, while the AM ratio has a more pronounced effect on sorptivity and GWP. The plots also highlight the importance of balancing both factors to achieve optimal performance in terms of desirability, tensile bond strength, and environmental impact.

The multi-criteria desirability analysis identifies the optimal parameters (molarity of 9.99 and AM ratio of 2.5) for achieving a balanced performance across all responses. Precise control over these parameters ensures accurate predictions and reliable experimental outcomes, confirming the robustness of the models.

3.8.5 Confirmation of Experiment

The confirmation of experiment analysis (Table 11) compares the predicted and observed values for compressive strength, sorptivity, shrinkage, tensile bond strength, and global warming potential (GWP), evaluated under a 95% confidence interval and a 99% population interval. For compressive strength, the predicted mean and median were both 14.5524, closely matching the observed value of 15.2100 and falling within the 95% confidence interval (CI) of 13.4866 to 15.6182, indicating accurate predictions. Similarly, for sorptivity, the predicted mean and median were 34.8004, with an observed value of 35.1200, fitting well within the 95% CI of 33.5533 to 36.0475, demonstrating the model's precision.

In the case of shrinkage, the predicted mean and median were 0.0027, closely aligning with the observed value of 0.0028 and within the 95% CI of 0.0024 to 0.0031, showing high model accuracy. For tensile bond strength, the predicted mean and median were 0.3655, with an observed value of 0.3700, fitting within the 95% CI of 0.3345 to 0.3964, indicating the model's efficacy. Finally, for GWP, the predicted mean and median were 261.3550, closely matching the observed value of 261.3500, and within the 95% CI of 260.5590 to 262.1510, confirming the model's reliability.

Overall, the observed values closely align with the predicted means and fall within the confidence and tolerance intervals, confirming the accuracy and reliability of the predictive models across all responses.

3.9 Microstructural Analysis

3.9.1 FESEM and EDX

Figure 24 presents the FE-SEM images of 10M2.5AM mixture exposed to heat curing at 60℃ for 24 h at 28 days of curing age. From the two images it could be observed that the heat-cured sample has a good compact microstructure which eventually influences the reported

Table 11 Comparison of predicted and observed values

Response	Predicted mean	Observed	Std Dev	SE mean	95% CI low for mean	95% CI high for mean	95% TI low for 99% pop	95% TI high for 99% pop
Compressive strength	14.5524	15.2100	1.5483	0.4711	13.4866	15.6182	7.1273	21.9775
Sorptivity	34.8004	35.1200	1.1817	0.5273	33.5533	36.0475	28.3306	41.2702
Shrinkage	0.0027	0.0028	0.0003	0.0001	0.0023	0.0030	0.0010	0.0044
Tensile bond	0.3654	0.3700	0.0293	0.0130	0.3345	0.3964	0.2048	0.5260
GWP	261.3550	261.3500	0.7543	0.3366	260.5590	262.1510	257.2260	265.4850

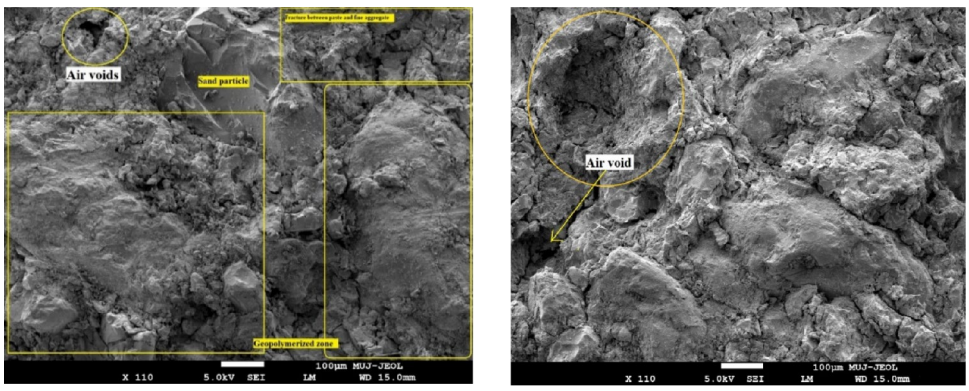

(a) (b)

Fig. 24 FESEM image of 10M2.5AM mixture cured at 60℃. **a** Low magnification, **b** high magnification

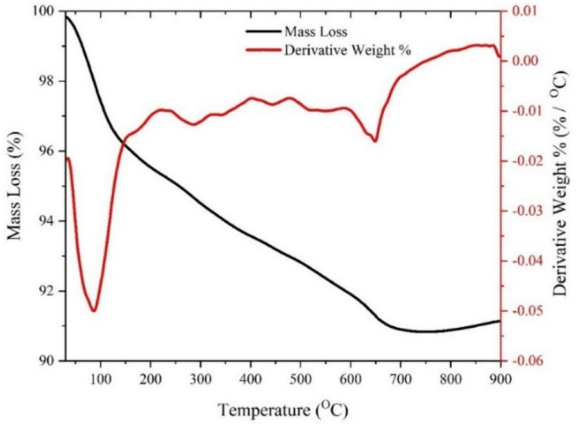

Fig. 25 Combined TGA and DTG graph for the 10M2.5AM sample after 28 days of curing at 60 ℃

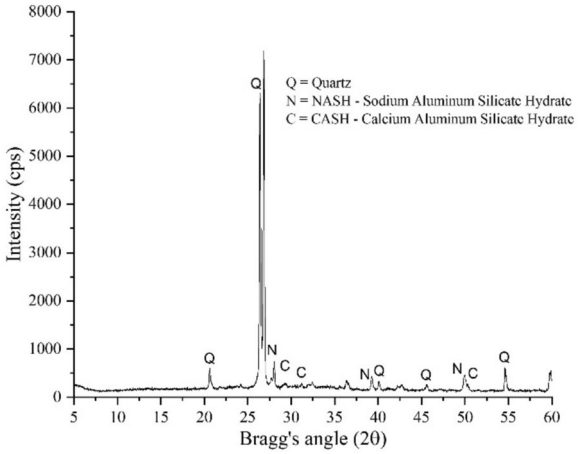

Fig. 26 Chemical compound identified in the 10M2.5AM sample

compressive strength, and the 10M2.5AM mixture was the highest among all the mixtures. However, images also reported multiple fracture lines with higher air voids which is due to shrinkage effect.

3.9.2 TGA

Figure 25 illustrates the TGA and DTG for the 10M2.5AM sample of 28 days curing age, cured at 60℃ for 24 h. From the DTG graph, it could be observed that the sample reported majorly two temperature zones of mass loss. The first mass loss zone is up to 250℃ from room temperature, and the second mass loss zone is at around 500–700℃. A slight peak at the DTG curve around 300–400℃ is also observed. Now the evaporation of physically bonded water and chemically bonded water (possible decomposition from the ettringite and other gels structures) results in the first peak at temperatures below 250 °C, as documented in the literature (Jochem et al., 2021). The second prominent peak, which occurred at temperatures between 500 and 700 ℃, alludes to calcite breakdown. Calcite is formed as a result of a possible carbonation reaction between reaction products and ambient CO_2 (I. Ismail et al., 2014). Further, the slight peak around 300–400 ℃ is associated with the dehydroxylation of the possible gel phases, like the presence of C-(A)-S–H gel.

3.9.3 XRD

Figure 26 presents the XRD analysis of 10M2.5AM mixtures. The presence of calcium in the precursor is responsible for forming the C-(A)-S–H gel along with the N-(A)-S–H gel. Though the peaks were shallow, which demonstrates that the formation of C-(A)-S–H is not the primary compound of geopolymers. The highest peaks for the N-(A)-S–H phase were identified at 27.883°, 39.201° and 49.753° with an intensity of 338, 451, and 231 while comparing with the JCPDS reference no. 00–018-1198 having the chemical formula as ($NaAlSi_3O_8 \cdot xH_2O$) and it is a form of zeolite. For the C-(A)-S–H phase, also commonly known as Zeolite X (Ca-based), bearing JCPDS reference no. 00-038-0232 with a chemical formula as $(Ca.Na).Al_2Si_{2.5}O_9.6.4H_2O$, is taken as a reference. The peaks are identified at 29.434°, 32.148° and 50.296° with an intensity of 267, 250, and 244.

4 2. Conclusions and Future Scope

This study investigated the use of waste cement concrete (WCC) as a precursor in geopolymer mortar production. The influence of varying molarity and alkaline mixture (AM) ratios on the physical, mechanical, environmental, and cost properties of the geopolymer mortar was studied. Compressive strength, shrinkage, tensile bond strength, sorptivity, and global warming potential (GWP) were evaluated. A multi-criteria analysis was performed to identify the optimal solution, balancing performance across all responses and the following conclusions were drawn based on the results and discussion:

- Based on the experimental investigation, the optimal conditions for the geopolymerization of waste cement concrete are identified as a 10 M NaOH solution with a 2.5 AM ratio, subjected to heat curing at 60 °C for 24 h. This combination yields approximately 80% of the 28-day compressive strength within the first 7 days, with long-term shrinkage stabilizing at 15–20% and reduced water absorption of 33.20 gm/100cm^2. The 12M2.5AM mixture achieved the highest tensile bond strength of 0.43 MPa at 90 days. Conversely, higher molarity and AM ratios increased shrinkage and void formation by up to 25%, adversely

impacting the mechanical and physical properties of the geopolymer mortar.

- The geopolymer mortar made from waste cement concrete demonstrates a lower global warming potential than conventional cement mortar, primarily due to the reduced energy consumption during production. Although the alkalis contribute significantly to the GWP in geopolymer mortars, they still exhibit an average 30% reduction compared to cement mortar. Geopolymer mortars also show a lower acidification potential, indicating a reduced environmental impact in terms of acidification. However, fossil fuel depletion is higher for geopolymer mortars due to the production of sodium hydroxide, with FF depletion increasing with the molarity of the mixtures. Overall, optimizing the alkali content and curing temperatures can enhance the environmental benefits of geopolymer mortars.
- The cost–benefit analysis reveals that geopolymer mortars generally offer better cost efficiency and sustainability than traditional cement mortars, especially with increased curing temperatures. Despite the additional cost of heat curing, most geopolymer mixtures achieve higher compressive strength and lower global warming potential, making them a more sustainable alternative. The ECM index for all criteria shows that all the geopolymers' scores are far better than the cement mortar. Among the geopolymers, the binary mixtures have the optimum score.

The multi-criteria desirability analysis identifies the optimal parameters (molarity of 10 and AM ratio of 2.5) for achieving a balanced performance across all responses. The precise control over these parameters ensures accurate predictions and reliable experimental outcomes, confirming the robustness of the models.

This study highlights a novel pathway for sustainable construction materials by studying the performance of WCC as a sole precursor material as geopolymer mortars. Hence from the study the following conclusions are drawn:

- The optimal conditions for geopolymerization were identified as a 10 M NaOH solution with a 2.5AM ratio, heat-cured at 60 ℃ for 24 h. This combination achieved 80% of the 28-day compressive strength within 7 days and demonstrated reduced water absorption and long-term drying shrinkage. Higher molarity and AM ratios adversely impacted the mechanical properties due to increased shrinkage and void formation.
- Geopolymer mortar made from WCC exhibited 30% lower global warming potential (GWP) compared to the conventional cement mortar, despite higher fossil fuel depletion due to sodium hydroxide production. Optimizing the alkali content and curing conditions enhances the environmental performance.
- A cost–benefit analysis indicated that geopolymer mortars are more cost efficient and sustainable than traditional cement mortar with increased curing temperature yielding better compressive strength and reduced GWP.
- Multicriteria desirability analysis by the use of central composite design to optimize molarity and alkaline ratios introduces a methodological innovation, enhancing performance predictability and advancing sustainability in construction. It also confirmed 10 M NaOH and 2.5AM ratio as the optimal parameters for balanced performance across all responses, ensuring accurate predictions and robust experimental outcomes.

The above outcomes will certainly solidify the potential of geopolymer mortars for broader application in the construction industry, however, several areas require further exploration and development to fully realize the potential of WCC-based geopolymer mortars. Few of them include long-term performance evaluations under varying environmental conditions, including freeze–thaw cycles and chemical exposures, are critical for assessing durability. Scaling up from laboratory production to industrial-scale applications presents challenges in maintaining material performance consistency, necessitating detailed investigations. Comprehensive economic assessments, encompassing lifecycle costs, long-term maintenance, and market feasibility, are vital for broader industry acceptance. Finally, policy integration is equally important, as the incorporation of geopolymer mortars into existing construction standards and regulations would enable widespread adoption.

Acknowledgements
We acknowledge MRC MNIT Jaipur, SAIF and CAF Lab of Manipal University Jaipur, and Graphic Era University for supporting this research.

Author contributions
MRM and SKD both contributed equally to conceptualizing the methodology, experimental and analytical investigations and writing the original draft. NG did the formal analysis of the literature review. SS helped in reviewing the original draft and supervision of the whole work. All authors read and approved of the final manuscript.

Funding
Open access funding provided by Manipal University Jaipur.

Availability of data and materials
The datasets used and/or analyzed during the current study are available from the corresponding author on reasonable request.

Declarations

Ethics approval and consent to participate

This study did not involve human or animal participants, so ethical approval and consent to participate were not applicable.

Consent for publication

All authors consent to the publication of this manuscript.

Competing interests

The authors declare that they have no competing interests.

Author details

[1]School of Engineering, NICMAR University, Pune 411045, Maharashtra, India. [2]Department of Civil Engineering, Manipal University Jaipur, Jaipur 303007, India. [3]Department of Civil Engineering, Graphic Era (Deemed to Be University), Dehradun 248002, India. [4]Department of Civil Engineering, Malaviya National Institute of Technology, Jaipur 302026, India.

Received: 12 September 2024 Accepted: 29 January 2025
Published online: 07 May 2025

References

Ahmari, S., Ren, X., Toufigh, V., & Zhang, L. (2012). Production of geopolymeric binder from blended waste concrete powder and fly ash. *Construction and Building Materials, 35*, 718–729. https://doi.org/10.1016/j.conbuildmat.2012.04.044

ASTM C1148. (2014). Standard Test Method for Measuring the Drying Shrinkage of Masonry Mortar. ASTM International, West Conshohocken, PA. https://doi.org/10.1520/C1148-92AR14.2

ASTM C1403. (2000). *Standard Test Method for Rate of Water Absorption of Masonry Mortars*.

BIS:2116. (1980). Specification for sand for masonry mortars. *Bureau of Indian Standards, New Delhi, India*, (Reaffirmed 2002), 1–13.

Bossink, B. A. G., & Brouwers, H. J. H. (1996). Construction waste: Quantification and source evaluation. *Journal of Construction Engineering and Management, 122*(1), 55–60. https://doi.org/10.1061/(ASCE)0733-9364(1996)122:1(55)

Brito, J. D. (2021). *Eco-Efficient Rendering Mortars*. Elsevier. https://doi.org/10.1016/C2018-0-04147-X

Buchwald, A., Hilbig, H., & Kaps, C. (2007). Alkali-activated metakaolin-slag blends—performance and structure in dependence of their composition. *Journal of Materials Science, 42*(9), 3024–3032. https://doi.org/10.1007/s10853-006-0525-6

Census of India. (2011). *Provisional Population Totals, Census of India 2011: Urban Agglomerations and Cities*. *Government of India*.

Das, S. K., & Shrivastava, S. (2021a). Influence of molarity and alkali mixture ratio on ambient temperature cured waste cement concrete based geopolymer mortar. *Construction and Building Materials, 301*(January), 124380. https://doi.org/10.1016/j.conbuildmat.2021.124380

Das, S. K., & Shrivastava, S. (2021b). Influence of molarity and alkali mixture ratio on ambient temperature cured waste cement concrete based geopolymer mortar. *Construction and Building Materials, 301*(July), 124380. https://doi.org/10.1016/j.conbuildmat.2021.124380

El-Wafa, M. A., & Fukuzawa, K. (2018). Early-age strength of alkali-activated municipal slag-fly ash-based geopolymer mortar. *Journal of Materials in Civil Engineering, 30*(4), 04018040. https://doi.org/10.1061/(ASCE)MT.1943-5533.0002234

Emission Standards: India,On-Road Vehicles and Engines. (n.d.). www.dieselnet.com. https://dieselnet.com/standards/in/

Farinha, C. B., Silvestre, J. D., de Brito, J., Veiga, M., & do R. (2019). Life cycle assessment of mortars with incorporation of industrial wastes. *Fibers, 7*(7), 59. https://doi.org/10.3390/fib7070059

Formoso, C. T., Soibelman, L., De Cesare, C., & Isatto, E. L. (2002). Material Waste in Building Industry: Main Causes and Prevention. *Journal of Construction Engineering and Management, 128*(4), 316–325. https://doi.org/10.1061/(ASCE)0733-9364(2002)128:4(316)

Ghazy, M. F. (2020). Optimization of recycled concrete aggregate geopolymer bricks by Taguchi Method. *REVISTA DE LA CONSTRUCCION, 19*(2), 244–254. https://doi.org/10.7764/RDLC.19.2.244

GOI-MOP. (2019). *CO2 baseline database for the Indian power sector user guide. Ministry of Power Govt of India* (Vol. 3).

Gomes, R., Silvestre, J. D., & de Brito, J. (2020). Environmental life cycle assessment of the manufacture of EPS granulates, lightweight concrete with EPS and high-density EPS boards. *Journal of Building Engineering, 28*, 101031. https://doi.org/10.1016/j.jobe.2019.101031

Görhan, G., & Kürklü, G. (2014). The influence of the NaOH solution on the properties of the fly ash-based geopolymer mortar cured at different temperatures. *Composites Part B: Engineering, 58*, 371–377. https://doi.org/10.1016/j.compositesb.2013.10.082

Hillier, S. R., Sangha, C. M., Plunkett, B. A., & Walden, P. J. (1999). Long-term leaching of toxic trace metals from Portland cement concrete. *Cement and Concrete Research, 29*(4), 515–521. https://doi.org/10.1016/S0008-8846(98)00200-2

Ismail, I., Bernal, S. A., Provis, J. L., San Nicolas, R., Hamdan, S., & Van Deventer, J. S. J. (2014). Modification of phase evolution in alkali-activated blast furnace slag by the incorporation of fly ash. *Cement and Concrete Composites, 45*, 125–135. https://doi.org/10.1016/j.cemconcomp.2013.09.006

Ismail, N., & El-Hassan, H. (2018). Development and characterization of fly ash-slag blended geopolymer mortar and lightweight concrete. *Journal of Materials in Civil Engineering, 30*(4), 1–14. https://doi.org/10.1061/(ASCE)MT.1943-5533.0002209

Ismail, S., & Ramli, M. (2013). Engineering properties of treated recycled concrete aggregate (RCA) for structural applications. *Construction and Building Materials, 44*, 464–476. https://doi.org/10.1016/j.conbuildmat.2013.03.014

Jiménez, C., Barra, M., Josa, A., & Valls, S. (2015). LCA of recycled and conventional concretes designed using the Equivalent Mortar Volume and classic methods. *Construction and Building Materials, 84*, 245–252. https://doi.org/10.1016/j.conbuildmat.2015.03.051

Jochem, L. F., Casagrande, C. A., Onghero, L., Venâncio, C., & Gleize, P. J. P. (2021). Effect of partial replacement of the cement by glass waste on cementitious pastes. *Construction and Building Materials, 273*, 121704. https://doi.org/10.1016/j.conbuildmat.2020.121704

Khodabakhshian, A., de Brito, J., Ghalehnovi, M., & Asadi Shamsabadi, E. (2018). Mechanical, environmental and economic performance of structural concrete containing silica fume and marble industry waste powder. *Construction and Building Materials, 169*(2018), 237–251. https://doi.org/10.1016/j.conbuildmat.2018.02.192

Komnitsas, K., Zaharaki, D., Vlachou, A., Bartzas, G., & Galetakis, M. (2015). Effect of synthesis parameters on the quality of construction and demolition wastes (CDW) geopolymers. *Advanced Powder Technology, 26*(2), 368–376. https://doi.org/10.1016/j.apt.2014.11.012

Lampris, C., Lupo, R., & Cheeseman, C. R. (2009). Geopolymerisation of silt generated from construction and demolition waste washing plants. *Waste Management, 29*(1), 368–373. https://doi.org/10.1016/j.wasman.2008.04.007

Lippiatt, B. C. (2000). *BEES 2.0 Building for Environmental and Economic Sustainability Technical Manual and User Guide*.

Malešev, M., Radonjanin, V., & Marinković, S. (2010). Recycled Concrete as Aggregate for Structural Concrete Production. *Sustainability, 2*(5), 1204–1225. https://doi.org/10.3390/su2051204

Marinković, S., Radonjanin, V., Malešev, M., & Ignjatović, I. (2010). Comparative environmental assessment of natural and recycled aggregate concrete. *Waste Management, 30*(11), 2255–2264. https://doi.org/10.1016/j.wasman.2010.04.012

Meshram, R. B., & Kumar, S. (2022). Comparative life cycle assessment (LCA) of geopolymer cement manufacturing with Portland cement in Indian context. *International Journal of Environmental Science and Technology, 19*(6), 4791–4802. https://doi.org/10.1007/s13762-021-03336-9

Najafi Kani, E., & Allahverdi, A. (2009). Effects of curing time and temperature on strength development of inorganic polymeric binder based on natural pozzolan. *Journal of Materials Science, 44*(12), 3088–3097. https://doi.org/10.1007/s10853-009-3411-1

Ortiz, O., Castells, F., & Sonnemann, G. (2009). Sustainability in the construction industry: A review of recent developments based on LCA. *Construction and Building Materials, 23*(1), 28–39. https://doi.org/10.1016/j.conbuildmat.2007.11.012

Parthiban, K., Mohan, S. R., & K. (2017). Influence of recycled concrete aggregates on the engineering and durability properties of alkali activated slag concrete. *Construction and Building Materials, 133*, 65–72. https://doi.org/10.1016/j.conbuildmat.2016.12.050

Poon, C. S., & Lam, C. S. (2008). The effect of aggregate-to-cement ratio and types of aggregates on the properties of pre-cast concrete blocks. *Cement and Concrete Composites, 30*(4), 283–289. https://doi.org/10.1016/j.cemconcomp.2007.10.005

Prakasan, S., Palaniappan, S., & Gettu, R. (2020). Study of Energy Use and CO2 Emissions in the Manufacturing of Clinker and Cement. *Journal of The Institution of Engineers (India): Series A*, *101*(1), 221–232. https://doi.org/10.1007/s40030-019-00409-4

Robayo-Salazar, R. A., Rivera, J. F., & Mejía de Gutiérrez, R. (2017). Alkali-activated building materials made with recycled construction and demolition wastes. *Construction and Building Materials, 149*, 130–138. https://doi.org/10.1016/j.conbuildmat.2017.05.122

Sagoe-Crentsil, K. K., Brown, T., & Taylor, A. H. (2001). Performance of concrete made with commercially produced coarse recycled concrete aggregate. *Cement and Concrete Research, 31*(5), 707–712. https://doi.org/10.1016/S0008-8846(00)00476-2

Singh, P. K., & Rajhans, P. (2024). Optimizing mechanical and durability properties of recycled aggregate concrete using pozzolanic slurries and modified mixing approach. *EUROPEAN JOURNAL OF ENVIRONMENTAL AND CIVIL ENGINEERING*. https://doi.org/10.1080/19648189.2024.2356019

United Nations. (2018). *World Urbanization Prospects 2018. Department of Economic and Social Affairs. World Population Prospects 2018.*

Yip, C. K., Lukey, G. C., & Van Deventer, J. S. J. (2005). The coexistence of geopolymeric gel and calcium silicate hydrate at the early stage of alkaline activation. *Cement and Concrete Research, 35*(9), 1688–1697. https://doi.org/10.1016/j.cemconres.2004.10.042

Zaharaki, D., Galetakis, M., & Komnitsas, K. (2016). Valorization of construction and demolition (C&D) and industrial wastes through alkali activation. *Construction and Building Materials, 121*, 686–693. https://doi.org/10.1016/j.conbuildmat.2016.06.051

Publisher's Note

Dr. Mohammed Rihan Maaze completed his Ph.D. from Malaviya National Institute of Technology (MNIT), Jaipur. He is working as an Assistant Professor in the School of Engineering at NICMAR University, Pune. Dr. Rihan received his M.Tech in Structural Engineering and earned a Gold Medal. He teaches Mechanics, Analysis, and Design subjects. Dr. Rihan has significantly contributed to sustainable construction materials, particularly in developing eco-friendly bricks from construction and demolition waste. This innovation earned him the prestigious SWACHH SARTHI Fellowship from Principal Scientific Advisor, Govt of India under the Waste to Wealth Mission. He has published twelve research articles in SCIE/ESCI-indexed journals and holds a patent on sustainable brick materials. Additionally, he serves as a reviewer for several respected journals.

Dr. Sourav Kumar Das is an Assistant Professor (Selection Grade) in the Department of Civil Engineering at Manipal University Jaipur, specialized in sustainable construction materials, concrete technology, and geopolymer research. His work primarily focuses on alkali-activated materials, waste-based cement alternatives, and artificial intelligence applications in civil engineering. With numerous publications in SCI/ESCI-indexed journals and patents in innovative material technologies, he actively contributes to advancing sustainable construction practices. His research aims to develop eco-friendly building materials while improving durability and efficiency in civil engineering applications.

Dr. Nikhil Garg completed his Ph.D. from Malaviya National Institute of Technology (MNIT), Jaipur, where he conducted research on eco-friendly rendering mortar incorporating recycled concrete and ceramic insulator waste. He is working as an Assistant Professor in the Department of Civil Engineering at Graphic Era (Deemed to be University), Dehradun, specializing in sustainable concrete technology, life cycle assessment (LCA), life cycle cost analysis (LCCA), and construction management. He received his M.Tech. in Construction Technology and Management from IIT Delhi and completed his B.Tech. in Civil Engineering from Graphic Era University, Dehradun. With over nine years of experience in academia and industry, he has been actively engaged in research, publishing multiple SCIE/ESCI-indexed journal articles, holding several design and utility patents on sustainable construction materials, and serving as a reviewer for reputed international journals.

Dr. Sandeep Shrivastava is an Associate Professor in the Department of Civil Engineering at Malaviya National Institute of Technology (MNIT) Jaipur. He specializes in sustainable materials and construction, focusing on the utilization of construction and demolition waste, life cycle assessment, and environmental product declarations. His research interests include sustainable materials and construction, construction and demolition waste, environmental product declarations, life cycle assessment, sustainability and circularity, greenhouse gas emissions and footprints, construction technology and management, and building information modelling.